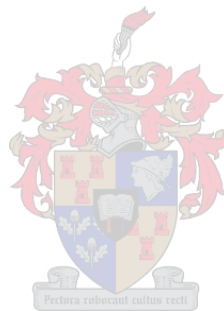# A QUANTUM HALL EFFECT WITHOUT LANDAU LEVELS IN A QUASI ONE DIMENSIONAL SYSTEM

By

Janetta Debora Brand

Thesis presented in partial fulfilment of the requirements for the degree of Master of Science at Stellenbosch University.

Supervisor : Doctor Izak Snyman

December 2012

DECLARATION

By submitting this thesis electronically, I declare that the entirety of the work contained therein is my own, original work, that I am the owner of the copyright thereof (unless to the extent explicitly otherwise stated) and that I have not previously in its entirety or in part submitted it for obtaining any qualification.

ABSTRACT

The experimental observation of the quantum Hall effect in a two-dimensional electron gas posed an intriguing question to theorists: Why is the quantization of conductance so precise, given the imperfections of the measured samples? The question was answered a few years later, when a connection was uncovered between the quantum Hall effect and topological quantities associated with the band structure of the material in which it is observed. The Hall conductance was revealed to be an integer topological invariant, implying its robustness to certain perturbations. The topological theory went further than explaining only the usual integer quantum Hall effect in a perpendicular magnetic field. Soon it was realized that it also applies to certain systems in which the total magnetic flux is zero. Thus it is possible to have a quantized Hall effect without Landau levels.

We study a carbon nanotube in a magnetic field perpendicular to its axial direction. Recent studies suggest that the application of an electric field parallel to the magnetic field would induce a gap in the electronic spectrum of a previously metallic carbon nanotube. Despite the quasi one-dimensional nature of the carbon nanotube, the gapped state supports a quantum Hall effect and is associated with a non zero topological invariant. This result is revealed when an additional magnetic field is applied parallel to the axis of the carbon nanotube. If the flux due to this magnetic field is varied by one flux quantum, exactly one electron is transported between the ends of the carbon nanotube.

OPSOMMING

Die eksperimentele waarneming van die kwantum Hall effek in 'n twee-dimensionele elektron gas laat 'n interessante vraag aan teoretiese fisikuste: Waarom sou die kwantisasie van die geleiding so presies wees al bevat die monsters, waarop die meetings gedoen word, onsuiwerhede? Hierdie vraag word 'n paar jaar later geantwoord toe 'n konneksie tussen die kwantum Hall effek en topologiese waardes, wat verband hou met die bandstruktuur van die monster, gemaak is. Dit is aan die lig gebring dat die Hall geleiding 'n heeltallige topologiese invariante is wat die robuustheid teen sekere steurings impliseer. Die topologiese teorie verduidelik nie net die gewone kwantum Hall effek wat in 'n loodregte magneetveld waargeneem word nie. Dit is ook moontlik om 'n kwantum Hall effek waar te neem in sekere sisteme waar die totale magneetvloed nul is. Dit is dus moontlik om 'n gekwantiseerde Hall effek sonder Landau levels te hê.

Ons bestudeer 'n koolstofnanobuis in 'n magneetveld loodreg tot die aksiale rigting. Onlangse studies dui daarop dat die toepassing van 'n elektriese veld parallel aan die magneetveld 'n gaping in die elektroniese spektrum van 'n metaliese koolstofnanobuis induseer. Ten spyte van die een-dimensionele aard van die koolstofnanobuis ondersteun die gapings-toestand steeds 'n kwantum Hall effek en hou dit verband met 'n nie-nul topologiese invariante. Hierdie resultaat word openbaar wanneer 'n bykomende magneetveld parallel tot die as van die koolstofnanobuis toegedien word. Indien die vloed as gevolg van hierdie magneetveld met een vloedkwantum verander word, word presies een elektron tussen die twee kante van die koolstofnanobuis vervoer.

ACKNOWLEDGEMENTS

I would like to acknowledge the contribution of the following people and institutions that made this work possible:

- My supervisor, Dr Izak Snyman, for his endless patience and guidance that helped me to develop an understanding of this subject.

- Jaco Bruwer and my parents, Floors and Retha Brand, who supported and encouraged me.

- The National Institute for Theoretical Studies for their financial support.

- My heavenly Father, who planned this interesting project to be part of my life journey.

CONTENTS

LIST OF FIGURES

CHAPTER 1
Introduction

1.1 Background

When an external magnetic field is applied perpendicularly to a current-carrying conductor, the moving charges experience a force, called the Lorentz force. This force causes the electrons to be deflected to one side of the conductor, so that a measurable voltage exists between the two sides of the conductor, as indicated in Figure 1.1. This is known as the classical Hall effect [1].
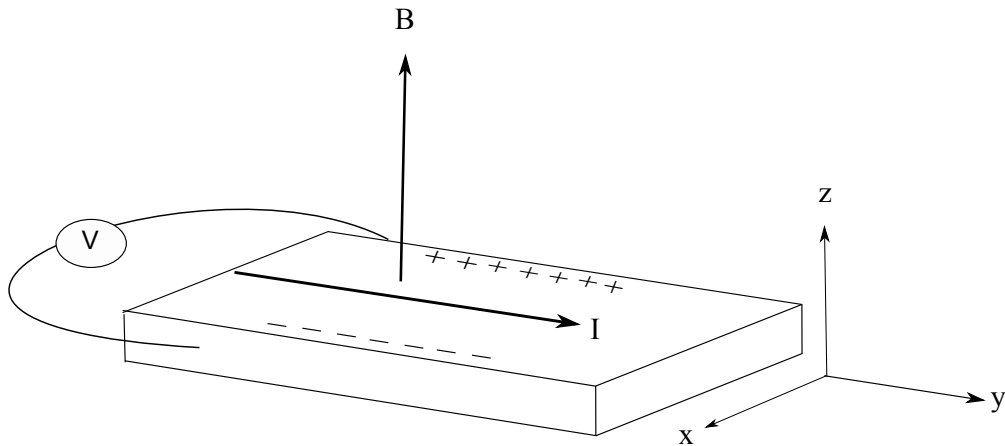
Figure 1.1: A conductor carrying current in the y direction. A magnetic field is applied in the z direction, perpendicular to the conductor. The magnetic field exerts a force on the electrons in the x direction. A measurable potential difference is created between the two sides.

The potential difference, V, due to the deflected electrons is proportional to the current I:

$$I = \sigma_{yx}V, \tag{1.1}$$

where, σ_{yx}, is a proportionality constant called the Hall conductance [2].

The quantum Hall effect can be thought of as a quantum mechanical version of the classical Hall effect. This effect is observed in two-dimensional electron systems exposed to low temperatures and high magnetic field strengths [3]. Here the Hall conductance is found to be quantized in units of e^2/h [4], [5]. This perfect quantization of the Hall conductance is one of the most remarkable experimental discoveries in condensed matter [6]. Making it even more intriguing is the fact that the measurement is robust and independent of microscopic details such as impurities in

the sample, electron-electron interactions or the exact value of the magnetic field [7]. This lead to the question: why is the quantization of conductance so precise, given the imperfections of the measured samples and experimental materials? Amongst the theoretical explanations, precipitated by this question, the Hall conductance has been realized to have topological significance [8], [9] and the precise quantization can be understood in terms of Chern numbers which are topological invariants, that does not change when small perturbations are added to the Hamiltonian [10].

The topological explanation for the robustness of the quantum Hall effect requires that the system has a non-degenerate ground state, and the ground state and the first excited state be separated by an energy gap. However, a gapped state does not guarantee a Hall effect. This can be understood by investigating the following two examples. Kane and Mele indicate that a gapped stated can be generated by spin-orbit interactions in a graphene sample without the need of an external magnetic field [11]. Although this example meets the requirement of a gapped state, the system will not experience a Hall effect, because time reversal symmetry is not broken. It does however support a spin-Hall effect. On the other hand, Haldane demonstrates that a gapped state can occur in the presence of a periodic magnetic field [12]. In this case a quantized Hall effect is experienced, even though the magnetic field is zero on average. Therefore, there are at least three restrictive physical conditions that a system must obey in order to be a positive candidate to experience a quantum Hall effect:

1. The ground state must be gapped.

2. Time reversal symmetry must be broken.

3. The system must be two-dimensional.

Graphene is a two-dimensional system composed of a single layer of carbon atoms. It was isolated in a laboratory for the first time in 2004, and since then it has been studied extensively, partly because of the material's extraordinary electron band structure. The unusual band structure give rises to a quantum Hall effect that can even observed at temperatures as high as room temperature [13]. The Hall effect that we refer to here is obtained in a constant magnetic field.

However, graphene can exhibit an even more exotic quantum Hall effect. Snyman investigated a graphene sheet in periodic magnetic and electric fields [14]. He found that a gapped ground state could be obtained when the position dependency of the electric field and the magnetic field were correlated. Furthermore, he indicated that the Hall conductance of the gapped ground

state was exactly $\pm e^2/h$. The topological theory only guarantees the Hall conductance to be equal to ne^2/h, with n$\in \mathbb{Z}$. The trivial case, when $n = 0$, is not excluded in the topological theory.

To apply periodic magnetic and electric fields to a graphene sheet is experimentally challenging. It is this challenge that inspired the present thesis. We shall now explain the system that we investigated. The experimental realization of this system, in terms of obtaining a magnetic field with zero spatial average, is more feasible than the system Snyman investigated.
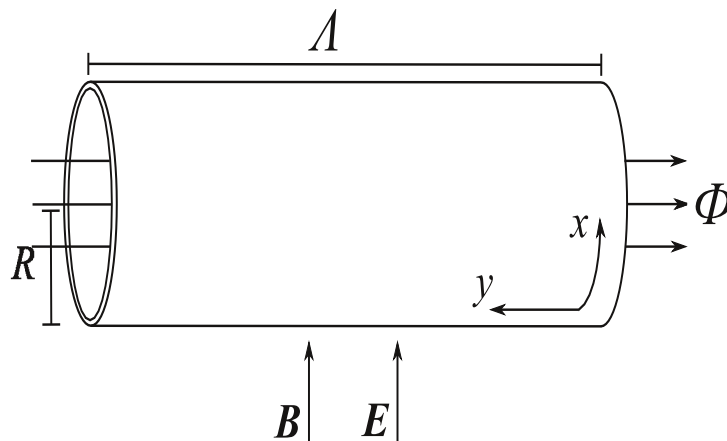
Figure 1.2:   A carbon nanotube in the presence of a constant magnetic field B and electric field E, parallel to each other and perpendicular to the tube axis. An additional magnetic field is applied parallel to the cylinder axis, in such a way that a magnetic flux Φ threads the tube. The length of the tube Λ, is much bigger than the radius R. The y-axis is chosen to point in the direction of the tube axis and the x-axis is chosen to be along the circumference.

We studied a carbon nanotube system to which we applied constant magnetic and electric fields perpendicular to the axis of the tube, as indicated in Figure 1.2. Because of the geometry, the applied magnetic and electric fields at the surface averaged out to zero around the circumference of the carbon nanotube. We chose a coordinate system such that the y-axis pointed in the direction of the tube axis and the x-axis around the circumference. Furthermore, we applied an additional magnetic field parallel to the axis of the tube. This magnetic field produces a flux, Φ, that threads the tube. From Faraday's law we know that when the flux varies, it produces an emf:

$$\varepsilon = -\frac{d\Phi}{dt}. \tag{1.2}$$

The final question that we shall answer in this thesis is: for a given electromotive force, what is

the current I that flows along the axis of the tube?

We take the same approach to our carbon nanotube system as Snyman did to the graphene sample. A carbon nanotube can viewed as a graphene sheet that is rolled into a cylinder. Inevitably there will be both similarities and differences between the carbon nanotube system and the graphene sample.

The first similarity between these two systems follows directly from the fact that a carbon nanotube is a 'graphene cylinder': the conductance electrons of both systems have the same properties and respond in similar ways to the applied magnetic and electric fields. The second similarity is that the electrons experience in both systems the same magnetic field with zero spatial average. If we apply a constant magnetic field perpendicular to the tube axis, they see a magnetic field that averages to zero around the circumference of the tube:

$$\boldsymbol{B} = B_0 \cos\left(\frac{2\pi x}{L}\right)\hat{z}, \tag{1.3}$$

so that there is, on average zero flux through the wall of the tube:

$$\int_0^L dx \boldsymbol{B}_z(x) = 0. \tag{1.4}$$

The same is valid for the electrostatic potential. The electrons of both system would see an electrostatic potential:

$$U = U_0 \cos\left(\frac{2\pi x}{L}\right), \tag{1.5}$$

that is correlated with the magnetic field.

The biggest difference between this nanotube system and the graphene system studied by Snyman is that the nanotube system is quasi one-dimensional, i.e. $x \in [0, L]$ and $y \in [-\infty, \infty]$, while the graphene system is two-dimensional, i.e. $x, y \in [-\infty, \infty]$. This characteristic (the fact that the carbon nanotube is one-dimensional) makes it a very interesting and exceptional system to study. In realistic systems the radius of the carbon nanotube, $R = L/2\pi$, is usually comparable to or smaller than other relevant length scales such as the magnetic length, $l_m = \sqrt{\hbar/eB}$, whereas the system investigated by Snyman is two-dimensional i.e. all relevant length scales are much smaller than the system size.

Why is the issue of one-dimension as opposed to two dimensions important? As stated before,

the quantization of the Hall conductance is explained in terms of topological invariants defined on the band structure of the first Brillouin zone, even in Snyman's work. This argument is only valid for a perfect, periodic two-dimensional crystal and cannot explain the quantization of a quasi one-dimensional system. However, there exists an alternative and less familiar argument that connects the Hall conductance with a topological invariant, provided by Niu, Thouless and Wu [15]. In this argument, the magnetic flux, Φ, plays the role that crystal momentum played in an argument mentioned before and given by Thouless, Kohmoto, Nightingale, and Den Nijs [8]. The argument, provided by Niu et al., predicts a quantized Hall conductance when edge effects can be ignored i.e. in situations where the observable in the bulk is independent of boundary values. This is the case when the system is much bigger than all the relevant length scales like $\hbar v_F/\text{gap}$ and the magnetic length, l_m. In the carbon nanotube system this is not always the case. The radius of the system is limited to a relatively small value. A quantized Hall conductance is not expected when the magnetic length is comparable to the radius of the tube. However, Niu et al.'s argument always guarantees quantized transport, even if the radius is smaller than the magnetic length, i.e. when the flux threading the tube is varied by one flux quantum, $\delta\Phi = h/e$, the number of electrons transported from the one end of the tube to the other is an integer. The argument of Niu et al., does not exclude the trivial case of zero electrons transported.

In this thesis we shall show that the ground state of the system in Figure 1.2 is gapped. We can therefore apply the argument used by Niu et al. Finally we can ask the question: how many electrons are transported from $y = 0$ to $y = \Lambda$ when Φ is varied by h/e. We show by analytical and numerical methods that the answer is one per spin.

1.2   Overview of this thesis

1.2.1   Chapter 2

Chapter 2 serves as a foundation on which the rest of the thesis is built. Both the quantum Hall effect and graphene have been studied extensively over decades and it would be impossible to present all these results. We only present the basic information needed to understand the following chapters.

We start of by explaining the hexagonal structure of the graphene lattice and introduce the tight binding Hamiltonian that describes the hopping of the electrons between nearest neighbors. The tight binding Hamiltonian is then used to calculate the interesting band structure of graphene. The system we study in this thesis is a carbon nanotube. It is therefore necessary to

explain how a graphene layer is rolled into a cylinder to form a carbon nanotube.

We introduce the quantum Hall effect in graphene. We examine the Landau level formation in a magnetic field perpendicular to the graphene sheet. By following Snyman's approach, we show that Landau levels can be formed in a graphene sample even though the magnetic flux is zero on average. This result leads to the expectation of a quantum Hall effect in our carbon nanotube system. Since this is a quasi one-dimensional system, we were forced to investigate the explanation given by Niu et al. for the quantization of the Hall conductance, rather than the more familiar explanation in terms of topological invariants defined on the band structure of the first Brillouin zone.

In the last part of this chapter we explicitly derive the velocity operators that appear in the Kubo formula. The Kubo formula is used to calculate the Hall conductance. We end this chapter by giving the Kubo formula in terms of single particle states. The Kubo formula expressed in terms of many body eigenstates and energies is convenient for studying the topological quantization of the Hall conductance, but the single particle version of the formula is more convenient for the calculations that we shall present in the next chapters.

1.2.2   Chapter 3

We show analytically that a gap in the band structure of a previously metallic carbon nanotube is induced at the Dirac point by applying an electric field parallel to a magnetic field that is perpendicular to the tube axis. Firstly we examine the gap formation for a toy model for which exact results for the energy spectrum can be obtained. We then show analytically that an electric field also induces a gapped state in realistic systems. We derive an expression for the Hall conductance when the Fermi energy is in the gap. It turns out that the system supports a quantum Hall effect, and when the flux of a magnetic field parallel to the tube axis is varied by one flux quantum, one electron is transported between the ends of the tube.

1.2.3   Chapter 4

For the analytical calculations of Chapter 3 we had to make certain assumptions. In Chapter 4 we test the accuracy and validity of the analytical results by comparing them with numerical results. We show explicitly how the nearest neighbor tight binding Hamiltonian is implemented in the numerical algorithm.

1.2.4   Chapter 5

In Chapter 5 we summarize al the conclusions reached in the previous chapters.

CHAPTER 2
Introduction to graphene and the quantum Hall effect

2.1   Basic physics of graphene

Graphene consists solely out of carbon atoms. This material may seem rather simple, but graphene turned out to be extremely interesting and captivated theorists attention for decades [12], [16], [17]. It was only recently that graphene had been isolated from graphite [18]. This experimental discovery lead to further theoretical investigations of this material and allowed experimentalists to test the extraordinary properties of graphene. This material has a number of interesting properties, mainly because of its hexagonal lattice structure and the unusual band structure.

We start off by explaining the structure of the graphene lattice. We discuss only the very basic definitions and background required for later chapters. The plan for the rest of the section is to study the nearest neighbor tight binding Hamiltonian that describes the dynamics of electrons on a honeycomb lattice in the presence of an electric field and a magnetic field. The tight binding Hamiltonian allows us to obtain the interesting band structure of graphene and we show that low energy excitations close to the Dirac points are described by a massless Dirac equation. Lastly we explain how the cylindrical structure of a carbon nanotube is obtained from a graphene sheet, because the system that we investigate is a carbon nanotube.

2.1.1   Lattice structure

Graphene is a single layer of carbon atoms arranged in a hexagonal lattice [19]. A hexagonal lattice can be represented as a Bravais lattice that contains two basis atoms [20]. These two basis atoms shall be referred to as A- and B-type atoms. It is important to realize that these two basis atoms are chemically identical. Later on we shall show that due to the two basis atoms, A and B, the energy spectrum has two energy bands - a valence band and a conduction band.

The position of any unit cell of the lattice is specified by $m\boldsymbol{a}_1 + n\boldsymbol{a}_2$, where $m, n \in Z$. The two primitive translation vectors $\boldsymbol{a_1}$ and $\boldsymbol{a_2}$ are given in terms of the lattice constant a, which is

8
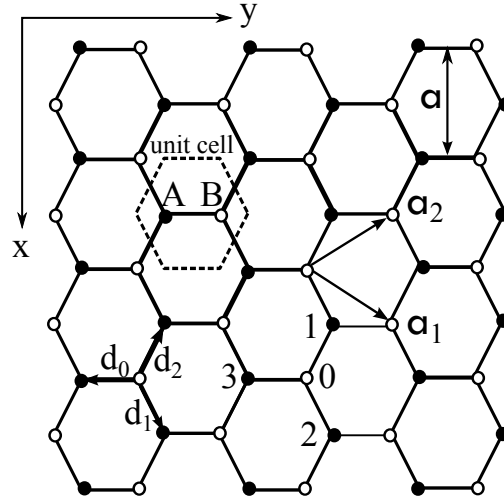
Figure 2.1: The hexagonal lattice structure of graphene, with the carbon atom represented by the black and white circles. Each unit cell contains two basis atoms, A and B and is represented by the dashed hexagonal line. The two primitive translation vectors are denoted as a_1 and a_2. The three vectors d_0, d_1 and d_2 are directed from a B site to its nearest neighbors, which are all A sites.

$\sqrt{3}$ times bigger than carbon-carbon separation distance $c = 0.142$ nm [21]. Explicitly they are:

$$\boldsymbol{a}_1 = a\left(\frac{1}{2}, \frac{\sqrt{3}}{2}\right), \tag{2.1a}$$

$$\boldsymbol{a}_2 = a\left(-\frac{1}{2}, \frac{\sqrt{3}}{2}\right). \tag{2.1b}$$

Each carbon atom in graphene has three nearest neighbors, for example the nearest neighbors of the carbon atom labeled 0 in Figure 2.1 are those labeled 1, 2 and 3. The graphene lattice is bi-partite, meaning that the three nearest neighbors of each A atom are all B atoms and *vice versa*. Furthermore, the three vectors connecting a B-type atom with its nearest neighbors, that are all A-type carbon atoms, are given by:

$$\boldsymbol{d}_0 = -a\left(0, \frac{1}{\sqrt{3}}\right), \tag{2.2a}$$

$$\boldsymbol{d}_1 = \frac{a}{2}\left(1, \frac{1}{\sqrt{3}}\right), \tag{2.2b}$$

$$\boldsymbol{d}_2 = \frac{a}{2}\left(-1, \frac{1}{\sqrt{3}}\right). \tag{2.2c}$$

The first Brillouin zone can be chosen to be a hexagon, as shown in Figure 2.2. Of the six vertices of the hexagonal Brillouin zone, only two are inequivalent, usually labeled as K and K':
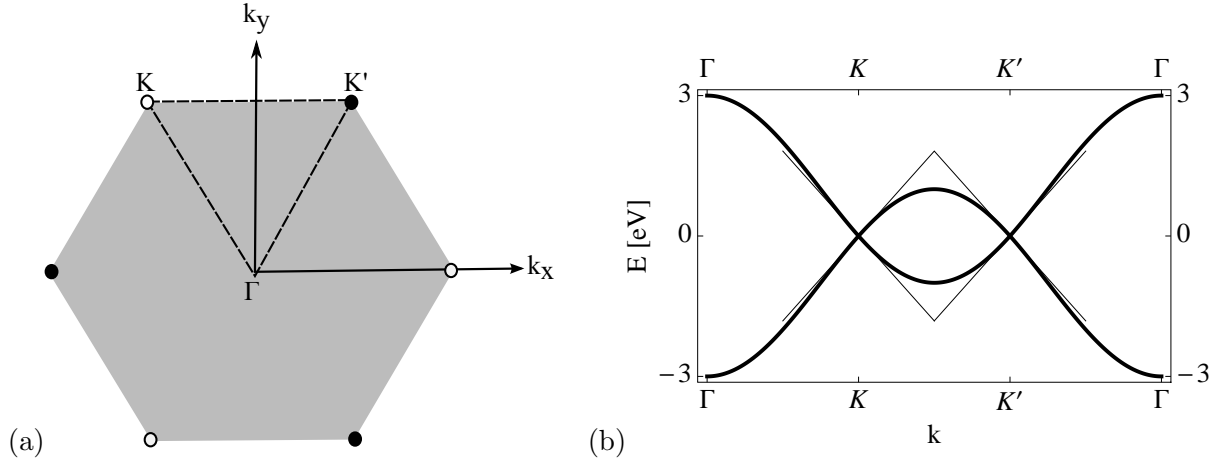
Figure 2.2: (a) The Brillouin zone of a two dimensional graphene lattice. The two K and K' points are inequivalent and are indicated at the vertices of the hexagon. The point Γ marks the center of the Brillouin zone. The dashed triangle in (a) is the contour that we follow to plot the energy dispersion in (b). The path is from the point Γ to the point K and from K to the point K' and then back to the center of the Brillouin zone. In (b) we see that the valence band and the conduction band touch exactly at energy equal to zero and at the two points K and K'.

$$K \;=\; \frac{2\pi}{a}\left(-\frac{1}{3},\frac{1}{\sqrt{3}}\right), \tag{2.3a}$$

$$K' \;=\; \frac{2\pi}{a}\left(\frac{1}{3},\frac{1}{\sqrt{3}}\right). \tag{2.3b}$$

The neighborhoods of these two points in the Brillouin zone are referred to as K and K' valleys. The relation $\boldsymbol{b}_i \cdot \boldsymbol{a}_j = 2\pi\delta_{ij}$ gives the basis vectors $\boldsymbol{b}_i$ of the reciprocal lattice that connects the three K points. The basis vectors, $\boldsymbol{b_1}$ and $\boldsymbol{b_2}$ are given by:

$$\boldsymbol{b}_1 \;=\; \frac{2\pi}{a}\left(1,\frac{1}{\sqrt{3}}\right), \tag{2.4a}$$

$$\boldsymbol{b}_2 \;=\; \frac{2\pi}{a}\left(-1,\frac{1}{\sqrt{3}}\right). \tag{2.4b}$$

In order to obtain the band structure of graphene, we now construct the nearest neighbor tight binding Hamiltonian for the graphene lattice.

2.1.2 Tight binding description

There is one free π-orbital per carbon atom in graphene. The delocalized electrons can hop between these orbitals [22]. The band structure of the graphene lattice is obtained by formulating

a tight binding Hamiltonian that allows one orbital for every lattice site. The simplest tight binding Hamiltonian that includes hopping between orbitals of nearest neighbor atoms, can be expressed as

$$H = H_0 + H_1, \tag{2.5}$$

where:

$$
\begin{aligned}
H_0 &= \sum_{m,n} U^{m,n} |m,n,X\rangle \langle m,n,X| \\
H_1 &= \sum_{m,n} t_0^{m,n} |m,n,B\rangle \langle m,n,A| \\
&+ \sum_{m,n} t_1^{m,n} |m+1,n,B\rangle \langle m,n,A| \\
&+ \sum_{m,n} t_2^{m,n} |m,n+1,B\rangle \langle m,n,A| + h.c.
\end{aligned}
\tag{2.6}
$$

Here X represents the A or B sublattice. The indices (m,n) refer to the unit cell at $m\boldsymbol{a}_1 + n\boldsymbol{a}_2$. The first part of the Hamiltonian (H_0) includes the electrostatic potential $U^{m,n}$ and the second part of the Hamiltonian (H_1) describes the hopping between the nearest neighbors, allowing spatial dependency of the hopping amplitudes;

$$t_j^{mn} = t e^{i\gamma_j^{mn}}, \tag{2.7}$$

where $j = 0, 1, 2$. The magnetic field $\boldsymbol{B} = \boldsymbol{\nabla} \times \boldsymbol{A}$, is incorporated in the three phases: γ_0^{mn}, γ_1^{mn} and γ_2^{mn} of the hopping amplitudes through the vector potential $\boldsymbol{A}$. The phases, in units of the flux quantum, must be chosen so that the total phase along any closed path is equal to the total enclosed magnetic flux. When the magnetic field is smooth on the scale of the lattice constant, each phase can be chosen so that they only depend on the vector potential $\boldsymbol{A}(\boldsymbol{r}_{mn})$ at unit cell (m,n).

It can be shown that any choice of the phases that satisfy

$$
A_x(\boldsymbol{r}_{mn}) = -\frac{\hbar}{ea}\left(\gamma_2^{mn} - \gamma_1^{mn}\right), \tag{2.8a}
$$

$$
A_y(\boldsymbol{r}_{mn}) = -\frac{2}{\sqrt{3}}\frac{\hbar}{ea}\left(\gamma_0^{mn} - \frac{\gamma_1^{mn}}{2} - \frac{\gamma_2^{mn}}{2}\right), \tag{2.8b}
$$

is valid. We choose:

$$\gamma_0^{mn} = -\frac{\sqrt{3}}{4}\frac{ea}{\hbar}A_y(\boldsymbol{r}_{mn}), \tag{2.9a}$$

$$\gamma_1^{mn} = \frac{\sqrt{3}}{4}\frac{ea}{\hbar}A_y(\boldsymbol{r}_{mn}) + \frac{ea}{2\hbar}A_x(\boldsymbol{r}_{mn}), \tag{2.9b}$$

$$\gamma_2^{mn} = \frac{\sqrt{3}}{4}\frac{ea}{\hbar}A_y(\boldsymbol{r}_{mn}) - \frac{ea}{2\hbar}A_x(\boldsymbol{r}_{mn}). \tag{2.9c}$$

We have constructed the nearest neighbor tight binding Hamiltonian, and can now proceed to obtain the band structure of the graphene lattice.

2.1.3 The bandstructure of graphene

To examine the bandstructure of graphene, we need to solve the tight binding Hamiltonian, Equation (2.6), with the vector potential $\boldsymbol{A}$ and the scalar potential U equal to zero and all three hopping amplitudes, $t_j^{m,n}$, equal to t. The measured value of t is $\simeq 2.66$ eV.

The two Bloch state wave functions, one for each of the two atoms in the unit cell of graphene are:

$$|\boldsymbol{k}, A\rangle = \frac{1}{\sqrt{N}}\sum_{m,n} e^{i\boldsymbol{k}\cdot\boldsymbol{r}_{mn}} |m, n, A\rangle, \tag{2.10a}$$

$$|\boldsymbol{k}, B\rangle = \frac{1}{\sqrt{N}}\sum_{m,n} e^{i\boldsymbol{k}\cdot\boldsymbol{r}_{mn}} |m, n, B\rangle, \tag{2.10b}$$

where $\boldsymbol{r}_{mn} = m\boldsymbol{a}_1 + n\boldsymbol{a}_2$ and $\boldsymbol{k}$ is a point in the first Brillouin Zone. The eigenstates of H have the form $a|\boldsymbol{k}, A\rangle + b|\boldsymbol{k}, B\rangle$. Substitution in Equation (2.6) yields:

$$t\begin{pmatrix} 0 & 1 + e^{i\boldsymbol{k}\cdot\boldsymbol{a}_1} + e^{i\boldsymbol{k}\cdot\boldsymbol{a}_2} \\ 1 + e^{-i\boldsymbol{k}\cdot\boldsymbol{a}_1} + e^{-i\boldsymbol{k}\cdot\boldsymbol{a}_2} & 0 \end{pmatrix}\begin{pmatrix} a \\ b \end{pmatrix} = \varepsilon(\boldsymbol{k})\begin{pmatrix} a \\ b \end{pmatrix}, \tag{2.11}$$

for a and b.

To evaluate the eigenvalues we substitute the primitive vectors of graphene, $\boldsymbol{a}_1$ and $\boldsymbol{a}_2$ into the equation above. After a short calculation, the eigenvalues are found to be:

$$\varepsilon(\boldsymbol{k}) = \pm|t|\sqrt{1 + 4\cos\left(k_y\frac{\sqrt{3}a}{2}\right)\cos\left(k_x\frac{a}{2}\right) + 4\cos^2\left(k_x\frac{a}{2}\right)}. \tag{2.12}$$

Some interesting and unusual properties emerge from the band structure, shown in Figure 2.2b. Firstly, the two atoms per unit cell give rise to two bands, namely the valence band and the conduction band. These two bands touch at six points, which are in fact the vertices of the Brillouin zone. In undoped graphene the Fermi energy is at $\varepsilon = 0$, exactly where the bands touch - these points are referred to as the Dirac points. As a result, the energy spectrum of graphene does not have a gap.

Another interesting feature is the shape of the valence band and the conduction band near the Dirac points. This is shown in Figure 2.2b and indicated with the thin black line. In these regions the energy spectrum of graphene is given by $\varepsilon = \pm v_F p$, where v_F is the Fermi velocity and $p = \sqrt{p_x^2 + p_y^2}$ is the momentum. This linear behavior is truly an amazing result, because it corresponds to the energy dispersion of massless Dirac fermions.

In the next section we study the electronic states in the vicinity of the Dirac points and show that the low-energy physics in graphene is described by the Dirac equation.

2.1.4 Low energy excitations and the Dirac equation for graphene

Low energy excitations are described by states in the vicinity of the Dirac points, K and K' and are found by expanding the wave functions around these points. We assume that the total wave function in position representation, for states in the vicinity of the Fermi energy, is given by:

$$\Psi_A(\boldsymbol{r}_{mn}) = e^{iK \cdot \boldsymbol{r}_{mn}} \phi_A^K(\boldsymbol{r}_{mn}) + e^{iK' \cdot \boldsymbol{r}_{mn}} \phi_A^{K'}(\boldsymbol{r}_{mn}), \tag{2.13a}$$

$$\Psi_B(\boldsymbol{r}_{mn}) = e^{iK \cdot \boldsymbol{r}_{mn}} \phi_B^K(\boldsymbol{r}_{mn}) + e^{iK' \cdot \boldsymbol{r}_{mn}} \phi_B^{K'}(\boldsymbol{r}_{mn}). \tag{2.13b}$$

Here $\phi_A^K(\boldsymbol{r})$, $\phi_B^K(\boldsymbol{r})$, $\phi_A^{K'}(\boldsymbol{r})$ and $\phi_B^{K'}(\boldsymbol{r})$ are slow-varying envelope functions, that are defined for all $\mathbb{R}^2$. The excitations around the Dirac points are found by expanding the momentum around K or K', to first order. [21] :

$$[v_F \boldsymbol{\sigma} \cdot (-\imath \hbar \partial_{\boldsymbol{r}} + e\boldsymbol{A}) + U]\Phi^Q = \varepsilon \Phi^Q, \tag{2.14}$$

where $Q = K$ or K' and

$$\boldsymbol{\Phi}^K(\boldsymbol{r}_{mn}) = \begin{bmatrix} \phi_A^K(\boldsymbol{r}_{mn}) \\ \phi_B^K(\boldsymbol{r}_{mn}) \end{bmatrix},\tag{2.15a}$$

$$\boldsymbol{\Phi}^{K'}(\boldsymbol{r}_{mn}) = \begin{bmatrix} -\phi_B^{K'}(\boldsymbol{r}_{mn}) \\ \phi_A^{K'}(\boldsymbol{r}_{mn}) \end{bmatrix}.\tag{2.15b}$$

Here $\boldsymbol{p} = -\imath\hbar(\partial/\partial x, \partial/\partial y)$ is the momentum operator, $\boldsymbol{A} = (A_x, A_y)$ is the vector potential and $v_F = \frac{\sqrt{3}}{2}\frac{at}{\hbar} \simeq 10^6 m/s$ the Fermi velocity which is proportional to the hopping parameter t and the lattice constant a. The Pauli matrices are represented by $\boldsymbol{\sigma} = (\sigma_x, \sigma_y)$, where:

$$\sigma_x = \begin{pmatrix} 0 & 1 \\ 1 & 0 \end{pmatrix},\tag{2.16a}$$

$$\sigma_y = \begin{pmatrix} 0 & -\imath \\ \imath & 0 \end{pmatrix}.\tag{2.16b}$$

Equation (2.14) bears a striking resemblance to the Dirac equation for massless neutrinos, also known as the Dirac-Weyl equation [23]. The low energy electrons in graphene therefore behave like massless Dirac fermions, but with the speed of light replaced by the Fermi velocity. A lot of research has been done on graphene because of this very interesting behavior and this property is considered as one of the most interesting characteristics of graphene.

2.1.5   Carbon nanotubes and the Dirac equation

Thus far we studied some interesting properties that an infinite graphene sheet exhibits. However, the system that we investigate is a carbon nanotube i.e. a graphene sheet rolled into a cylinder. We now explain how to construct a single wall carbon nanotube from a graphene lattice.

We define the chiral vector,

$$\boldsymbol{L} = n\boldsymbol{a}_1 + m\boldsymbol{a}_2,\tag{2.17}$$

that specifies how the graphene sheet is rolled up. This is illustrated in Figure 1.3. A carbon nanotube is constructed such that the hexagon at $\boldsymbol{L}$, (n, m), is rolled onto the hexagon at the
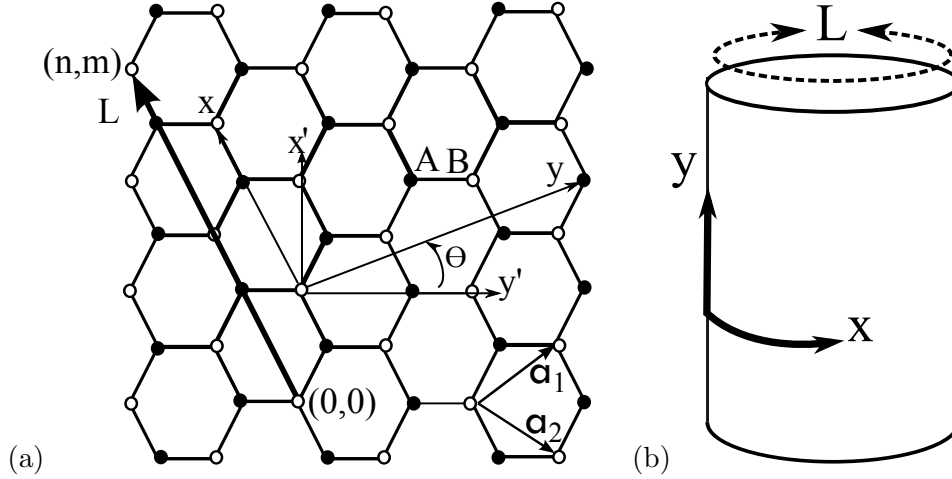
Figure 2.3: **(a) The construction of the carbon nanotube corresponds to the chiral vector** $\boldsymbol{L}$**. The** x **and** y **coordinates run along the circumference and the axis of the tube respectively. The position of** x' **and** y' **is fixed with respect to the lattice structure. (b) The** x **and** y **coordinates in the carbon nanotube.**

origin, (0,0). The circumference is therefore equal to the length of the chiral vector,

$$L = |\boldsymbol{L}| = a\sqrt{n^2 + m^2 + \frac{1}{4}mn}. \tag{2.18}$$

As shown in the previous section, the low energy electrons in graphene are described by the Dirac equation. Therefore, the Dirac equation describes also the low energy electrons in a carbon nanotube and is given by:

$$[v_F \boldsymbol{\sigma} \cdot (-\imath\hbar\partial_{\boldsymbol{r}} + e\boldsymbol{A}) + U]\Phi = \varepsilon\Phi. \tag{2.19}$$

The co-ordinate system is chosen such that the y-axis is parallel to the tube axis, and the x-axis runs around the circumference, as in Figure 2.3. The boundary condition for both the K and K' valley, as described by Ando [24], is given by

$$\Psi^K(\boldsymbol{r} + L\hat{\boldsymbol{x}}) = e^{-\imath K \cdot L}\Psi^K(\boldsymbol{r}) = e^{i(\theta - 2\pi\nu/3)}\Psi^K(\boldsymbol{r}), \tag{2.20a}$$

$$\Psi^{K'}(\boldsymbol{r} + L\hat{\boldsymbol{x}}) = e^{-\imath K' \cdot L}\Psi^{K'}(\boldsymbol{r}) = e^{i(\theta + 2\pi\nu/3)}\Psi^{K'}(\boldsymbol{r}). \tag{2.20b}$$

The phase θ, in Equation (2.20) takes into account the effect of a magnetic field that is parallel with the axis of the carbon nanotube and is given by

$$\theta = 2\pi\Phi/\phi_0. \tag{2.21}$$

Here Φ is the flux through the cross section of the tube and ϕ_0 is the magnetic flux quantum given by $\phi_0 = h/e$, where e is the elementary charge and h is Planck's constant.

The integer ν assumes values of 0 or ± 1 and is determined by the relation:

$$n + m = 3N + \nu, \tag{2.22}$$

where N is an integer. Ando shows that when $\theta = 0$ and $\nu = 0$, the conduction and valence band cross and the nanotube is therefore metallic, whereas when $\theta = 0$ and $\nu = \pm 1$ there is a nonzero gap between the conduction band and valence band and the tube is semi-conducting.

2.2   The Quantum Hall effect

The quantum Hall effect is a striking phenomenon observed in two-dimensional electron systems subjected to strong magnetic fields and low temperatures. This phenomenon is remarkable, because of the exact quantization that the Hall conductance exhibits in these systems. The Hall conductivity is defined as the ratio of the transverse potential difference to the total current, as explained in the beginning of Chapter 1, Equation (1.1). When the Hall conductance is plotted against the magnetic field perpendicular to the system, the plot exhibits plateau regions. These flat regions are evidence of the quantization of the Hall conductivity, with values:

$$\sigma_{yx} = \nu \frac{e^2}{h}. \tag{2.23}$$

Here e is the elementary charge, h is Planck's constant and ν can take on either integer values or values that are rational fractions. Depending on whether ν is an integer or a fraction, we refer to this effect as the integral quantum Hall effect (IQHE) or the fractional quantum Hall effect (FQHE). The IQHE can be described in terms of the kinetic-energy quantization of independent electrons in a magnetic field, whereas the FQHE is not as straight forward, because here the interaction between the electrons play a crucial role. In this thesis we will exclusively focus on the IQHE.

In 1985 Klaus von Klitzing was awarded the Nobel prize in physics for his experimental discovery of the quantum Hall effect. Von Klitzing's discovery that the Hall conductance is exactly quantized, resulted from predictions made by Ando, Matsumoto and Uemura in 1975 [25]. The experimental result was quite remarkable and the *precise* quantization of the Hall conductance

came as a big surprise to both theoretical and experimental physicists. We would expect to have corrections of various sorts, resulting for example from electron-electron interactions, impurities, substrate potentials, etc., but it was found that the result is robust against these effects.

The precise quantization of the experimental results posed an intriguing puzzle to theorists and soon a successful theory was put forward. Probably the most elegant formulation of this theory involves the concept of algebraic topology. In this approach the Hall conductance is expressed as a topological invariant called a Chern number - which is always an integer. The relevance of this fact is that a topological invariant does not change when the manifold, on which it is defined, is continuously deformed.

Graphene is an ideal two-dimensional system in which the quantum Hall effect has been observed [34]. The electronic properties of graphene give rise to a very unique quantum Hall effect that is different from the quantum Hall effect observed in other two dimensional systems. We shall explicitly show these differences, by studying the Landau level formation when a magnetic field is placed perpendicular to the graphene sheet.

We also investigate a graphene sheet subjected to a magnetic field with zero spatial average. This is relevant to our study, because the system that we investigate is also subjected to a magnetic field that is periodic in space. Snyman prove that it is possible to achieve a quantum Hall effect in a graphene sample where the magnetic flux is zero on average [14]. We follow his calculations and show that a electric field parallel to the magnetic field induces a gap in the band structure of graphene. We shall see that the electrons experience a magnetic field even though they are subjected to a magnetic field with zero spatial average. This result gives us reason to believe that a non zero quantum Hall effect is also expected in the carbon nanotube system.

However, due to the quasi one-dimensional nature of the carbon nanotube system, we can not explain the quantization of the Hall conductance in terms of topological invariants defined on the band structure of the first Brillouin zone. We need another explanation, such a explanation exists and is discussed in the last part of this section.

2.2.1   Landau energy levels of graphene: Constant magnetic field

Since the best known realizations of the quantum Hall effect occur in a constant magnetic field, we investigate the energy levels of a single graphene layer in a magnetic field that is con-

stant in space. Let the graphene layer be in the xy-plane and the magnetic field be perpendicular to this plane. We firstly choose a gauge for the vector potential. The vector potential is then substituted in the Dirac equation and the energy levels are calculated.

A possible choice for the vector potential, corresponding to the magnetic field $B\hat{z}$, would be the so-called Landau gauge

$$\boldsymbol{A}(\boldsymbol{r}) = Bx\hat{\boldsymbol{y}}. \tag{2.24}$$

The Dirac Hamiltonian in terms of this choice for the vector potential is given by

$$[v_F\boldsymbol{\sigma}\cdot(-\imath\hbar\partial_{\boldsymbol{r}} + eBx\hat{\boldsymbol{y}})]\Psi^Q = E\Psi^Q, \tag{2.25}$$

where Q labels the valleys K and K', so that

$$\Psi^K(\boldsymbol{r}) = \begin{pmatrix} \psi_A^K(\boldsymbol{r}) \\ \psi_B^K(\boldsymbol{r}) \end{pmatrix}, \tag{2.26a}$$

$$\Psi^{K'}(\boldsymbol{r}) = \begin{pmatrix} -\psi_B^{K'}(\boldsymbol{r}) \\ \psi_A^{K'}(\boldsymbol{r}) \end{pmatrix}. \tag{2.26b}$$

The equations that describe the K and K' valleys respectively are decoupled and we can therefore solve them separately. We start by finding the solutions for the K valley. The method that we use to solve the Dirac equation, $H\Psi^K = E\Psi^K$, is separation of variables. We substitute the wave function $\Psi^K(\boldsymbol{r})$, with a wave function of the form

$$\Psi^K(\boldsymbol{r}) = e^{\imath ky}\psi^K(x), \tag{2.27}$$

into the Dirac equation, Equation (2.14). This leads to the equation

$$E\psi^K(x) = -\imath\hbar v_F \begin{pmatrix} 0 & \partial_x + k + \frac{e}{\hbar}Bx \\ \partial_x - k - \frac{e}{\hbar}Bx & 0 \end{pmatrix} \psi^K(x). \tag{2.28}$$

Written in terms of the components ψ_A^K and ψ_B^K we have

$$E\psi_A^K(x) = -\imath\hbar v_F \left(\partial_x + k + \frac{eB}{\hbar}x \right) \psi_B^K(x), \tag{2.29a}$$

$$E\psi_B^K(x) = -\imath\hbar v_F \left(\partial_x - k - \frac{eB}{\hbar}x \right) \psi_A^K(x). \tag{2.29b}$$

Substituting the magnetic length

$$l_m = \sqrt{\frac{\hbar}{eB}}, \tag{2.30}$$

into the equations above we obtain

$$E\psi_A^K(x) = -\imath\hbar\upsilon_F \left[\partial_x + \left(\frac{1}{l_m}\right)^2 \left(l_m^2 k + x\right)\right] \psi_B^K(x), \tag{2.31a}$$

$$E\psi_B^K(x) = -\imath\hbar\upsilon_F \left[\partial_x - \left(\frac{1}{l_m}\right)^2 \left(l_m^2 k + x\right)\right] \psi_A^K(x). \tag{2.31b}$$

These equations can be decoupled by substituting the one equation into the other, so that

$$E^2\psi_A^{\boldsymbol{K}}(x) = (\hbar\upsilon_F)^2 \left[-\partial_x^2 + \left(\frac{1}{l_m}\right)^2 + \left(\frac{1}{l_m}\right)^4 \left(x + l_m^2 k\right)^2\right] \psi_A^{\boldsymbol{K}}(x), \tag{2.32a}$$

$$E^2\psi_B^{\boldsymbol{K}}(x) = (\hbar\upsilon_F)^2 \left[-\partial_x^2 - \left(\frac{1}{l_m}\right)^2 + \left(\frac{1}{l_m}\right)^4 \left(x + l_m^2 k\right)^2\right] \psi_B^{\boldsymbol{K}}(x). \tag{2.32b}$$

Equation (2.32b) can be rewritten as

$$\left[\frac{1}{2}\left(\frac{E}{\hbar\upsilon_F}\right)^2 + \frac{1}{2}\left(\frac{1}{l_m}\right)^2\right] \psi_B(x) = \left[-\frac{1}{2}\partial_x^2 - \frac{1}{2}\left(\frac{1}{l_m}\right)^4 \left(x + l_m k\right)^2\right] \psi_B(x). \tag{2.33}$$

It is now easy to see that the right side of Equation (2.33) has the form of a one-dimensional displaced Harmonic oscillator that is oscillating around the position $x_0 = l_m k$. The eigenvalues for this one-dimensional oscillator is $\left(n + \frac{1}{2}\right)/l_m^2$, with $n = 0, 1, 2, ...$ so that

$$\frac{1}{2}\left(\frac{E}{\hbar\upsilon_F}\right)^2 + \frac{1}{2}\left(\frac{1}{l_m}\right)^2 = \left(n + \frac{1}{2}\right)\frac{1}{l_m^2}. \tag{2.34}$$

In a constant magnetic field the energy spectrum for Equation (2.33) is therefore quantized at energies:

$$E = \text{sgn}(n)\sqrt{n}\hbar\omega_c, \tag{2.35}$$

where $n = 0, \pm 1, \pm 2...$ is the Landau index and $\omega_c = \frac{\sqrt{2}\upsilon_F}{l_m} = \upsilon_F\sqrt{\frac{2eB}{\hbar}}$ the cyclotron frequency that is proportional to $\sqrt{B}$. The energy levels are known as the Landau levels. Note that, since the energy does not depend on k, the wave number in the y-direction, each Landau level is infinitely degenerate (at least in an infinite sample). The positive energy values corresponds to the conduction band and the negative values corresponds to the valence band. Furthermore, the

Landau levels are unevenly spaced, with the largest space between subsequent Landau levels is between the zeroth and the first Landau level.

This result differs from Schrödinger electrons. The Landau levels for Schrödinger electrons are evenly spaced, with the spacing between each level equal to $\hbar eB/m^*$. The effective mass m^* can be significantly less than the true electron mass. We now compare the biggest gap between Landau-levels in graphene with a Landau level gap in GaAs with an effective mass, $m^* = 0.07 m_e$.

- For GaAS: $\Delta E(\text{in eV}) = 1.5 \times 10^{-3} B \,(\text{in Tesla})$.

- For graphene: $\Delta E(\text{in eV}) = 3.5 \times 10^{-2} \sqrt{B(\text{in Tesla})}$.

To observe the quantum Hall effect at room temperature, $\Delta E/k_B$ must be bigger than $\sim 10^3$ Kelvin, that is to say $\Delta E \gtrsim 10^{-1}$ eV. Consequently, in graphene a 10 Tesla field is sufficient, but to observe the quantum Hall effect, while in GaAs, a 66 Tesla field is required. It is this large gap between the valence band and the conduction band that enables us to observe the quantum Hall effect in graphene, even at temperatures as high as room temperature.

To calculate the energy levels for Equation (2.32a), we repeat the procedure and find

$$E = \pm \sqrt{n+1}\hbar\omega_c, \tag{2.36}$$

for $n = 0, 1, 2, \ldots$. Comparing this result with the result obtained for Equation (2.32b) we notice that here the level at $E = 0$ is absent. The implication of this is that for both the sub-lattices A and B the wavefunction have non-zero amplitudes at the Landau levels where $n \neq 0$, while at the Landau level $n = 0$ the wavefunctions have a non-zero amplitude only for the B sub-lattice.

The same analysis can be performed for the K' valley. Here the roles of the A and B sublattice are reversed. Combining the results for the K and K' valleys, one finds that each Landau level is valley degenerate.

2.2.2 Periodic magnetic field

We now investigate a graphene sheet subjected to a magnetic field that is periodic in space. The reason for this discussion is that the system we investigate is also subjected to a magnetic field with zero spatial average. Here we follow the same approach as Snyman and show that it is possible to create a gap between the valence band and the conduction band even though the

magnetic flux is zero on average [14].

The zero energy solutions for a graphene layer in a periodic oscillating magnetic field can be calculated exactly. Here we present only the results, later on we show the calculation for a similar example in more detail.

The magnetic field that we consider is also perpendicular to the graphene layer as in the previous example, but here we choose it to be periodic in space and so that the average flux through the sample is zero. The periodicity of the magnetic field can be described in terms of a Bravais lattice with two primitive unit cell basis vectors $\boldsymbol{a}_k$, with $k = 1, 2$, so that $B(\boldsymbol{r} + \boldsymbol{a}_k) = B(\boldsymbol{r})$. This is not the same lattice as that of the underlying graphene. We refer to this unit cell as UC. The Fourier components of the magnetic field are given by

$$B_{mn} = l^{-2} \int_{UC} d^2 r \, e^{-\imath \boldsymbol{k}_{mn} \cdot \boldsymbol{r}} B(\boldsymbol{r}), \tag{2.37}$$

where $\boldsymbol{k}_{mn} = m\boldsymbol{b}_1 + n\boldsymbol{b}_2$ and $\boldsymbol{b}_j$, $j = 1, 2$ are the basis vectors of the reciprocal lattice. We assume that the graphene sample is very large in comparison to the UC so that we only consider the bulk effects. For convenience we impose the following periodic boundary conditions:

$$\Psi(\boldsymbol{r}) = \Psi(\boldsymbol{r} + \boldsymbol{\Omega}_k), \tag{2.38}$$

with $\boldsymbol{\Omega}_k = M_k \boldsymbol{a}_k$, where M_k for $k = 1, 2$ are large integers. In the Coulomb gauge, where $\partial_{\boldsymbol{r}} \cdot \boldsymbol{A} = 0$, it is easily verified that the zero-energy eigenstates of the Dirac Equation (2.14) are

$$\Psi_{+,0}(x) = \frac{N_+}{\Omega} \begin{pmatrix} e^{F(x)} \\ 0 \end{pmatrix}, \tag{2.39a}$$

$$\Psi_{-,0}(x) = \frac{N_-}{\Omega} \begin{pmatrix} 0 \\ e^{-F(x)} \end{pmatrix}. \tag{2.39b}$$

The function F is defined in terms of the Fourier components B_{mn} of the magnetic field and is given by

$$F(\boldsymbol{r}) = -\frac{e}{\hbar} \sum_{mn \neq 0} \frac{B_{m,n}}{|\boldsymbol{k}_{mn}|^2} e^{\imath \boldsymbol{k}_{mn} \cdot \boldsymbol{r}}, \tag{2.40}$$

and satisfies

$$\partial_{\boldsymbol{r}}^2 F = \frac{eB}{\hbar}. \tag{2.41}$$

N_+ and N_- are the normalization constants:

$$N_\pm = \left[\int_{UC} d^2r \, e^{\pm 2F(\boldsymbol{r})} \right]^{-1/2}. \tag{2.42}$$

$$\tag{2.43}$$

For the K valley, $\Psi_{+,0}$ is A sublattice polarized and $\Psi_{-,0}$ is B sublattice polarized. In the K' valley the roles of the sublattices are reversed and consequently, $\Psi_{-,0}$ is A sublattice polarized and $\Psi_{+,0}$ is B sublattice polarized.

We can show that the sign of the function F is anticorrelated with the direction of the magnetic field. We define P as follows:

$$P = \frac{e}{\hbar} \int_{UC} d^2r \, B(\boldsymbol{r}) F(\boldsymbol{r}), \tag{2.44}$$

When P is negative, the function $F(\boldsymbol{r})$ is anticorrelated with $B(\boldsymbol{r})$. From Equation(2.41) follows:

$$P = \int_{UC} d^2r \, B(\boldsymbol{r}) \partial_r^2 B(\boldsymbol{r}). \tag{2.45}$$

Using Gauss's theorem and integration by parts, the integral can be written as:

$$P = \int_{\partial UC} d\boldsymbol{r}_\perp \cdot B \partial_r B - \int_{UC} d^2r \, |\partial_r B|^2. \tag{2.46}$$

The integration in the first term runs over the boundary of UC, with $d\boldsymbol{r}_\perp$ normal to the boundary and pointing outwards. This term turns out to be equal to zero because B is periodic on UC. P is therefore negative. This means the sign of F is anticorrelated with the direction of the magnetic field and that F tends to be negative in regions where the magnetic field points in the positive $\boldsymbol{z}$-direction and positive in regions where the magnetic field points in the negative $\boldsymbol{z}$-direction.

In order to observe a Hall effect, a gap in the spectrum must be induced. This can be achieved by applying an electric field parallel to the magnetic field. The result of a scalar potential U, with a spatial profile correlated with the spatial profile of the magnetic field, is that the energy of the state $\Psi_{-,0}$ is raised and the energy of the state $\Psi_{+,0}$ is lowered. The opposite occurs if the spatial profile of the scalar potential is anticorrelated with the spatial profile of the magnetic field, i.e. the energy of the state $\Psi_{+,0}$ is raised and the energy of the state $\Psi_{-,0}$ is lowered.

In the presence of a weak periodic scalar potential, the energies near zero can be calculated perturbatively. The result is

$$E = \pm\sqrt{(\hbar\tilde{v}_F|\boldsymbol{k}|)^2 + \mu^2}. \tag{2.47}$$

Here v_F is the renormalized Fermi velocity

$$\tilde{v}_F = l^2 N_+ N_- v_F, \tag{2.48}$$

and μ the effective mass is given by

$$\mu = \frac{1}{2}\int_{UC} U(\boldsymbol{r})(N_+^2 e^{2F(\boldsymbol{r})} - N_-^{-2F(\boldsymbol{r})}). \tag{2.49}$$

The gap between the valence band and the conduction band is equal to 2μ. Therefore, when an electric field is applied parallel to the magnetic field, the electrostatic potential induces a gap between the valence band and the conduction band.

When $\mu > 0$, the highest valence band states are similar to $\Psi_{-,0}$ and therefore represents the particles that are localized where the magnetic field is positive. When $\mu < 0$, the highest valence band states are equal to $\Psi_{+,0}$ and represents particles localized where the magnetic field is negative. However, in both cases the valence band electrons experience a magnetic field with a well defined polarity. Based on the results in a constant field, it is therefore plausible to expect a non-zero Hall effect, which is indeed the case when a calculation is carried out.

2.2.3 Quasi one-dimensional system and topologically invariant.

Due to the quasi one-dimensional nature of the carbon nanotube system, the quantization of the Hall conductance cannot be be explained in terms of topological invariants defined on the band structure of the first Brillouin zone. This argument is only possible for a perfect, periodic two-dimensional structure such as a two-dimensional crystal without impurities. However, a theory that under certain conditions explains the perfect quantization of the Hall effect and does not refer to the band structure of a perfect crystal exists [15]. The theory requires that the Fermi energy lies within a gap and the ground state is nondegenerate. Furthermore, the system should be large enough so that there is no response in the bulk of the sample to a perturbation at its edge. We briefly review the argument of Niu et al.
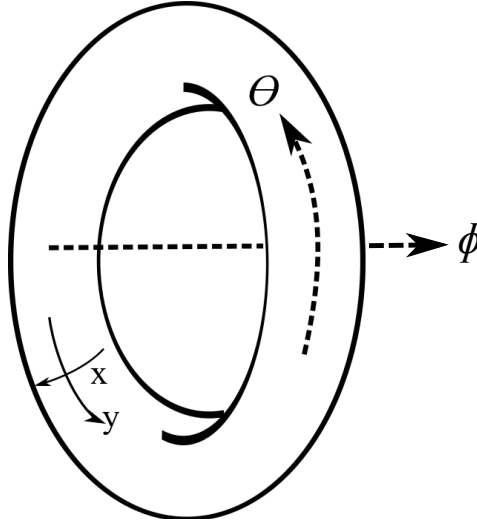
Figure 2.4: A torus representing a carbon nanotube subjected to a magnetic flux in the x- and y-direction as indicated.

The carbon nanotube that we investigate are long enough so that the boundary condition in the longitudinal direction does not effect the results. The carbon nanotube can therefore be placed on a torus by joining the two ends of the tube. We apply two fluxes, θ and ϕ to the torus such that the torus experiences a flux $\theta h/e$ through any cross section along the x-direction and a flux $\phi h/e$ through any cross section along the y-direction. This is illustrated in Figure 2.4. The total vector potential of the system is equal to:

$$\boldsymbol{A}_{total} = \boldsymbol{A} - \frac{\hbar}{e}\frac{\theta}{L_1}\hat{\boldsymbol{x}} - \frac{\hbar}{e}\frac{\phi}{L_2}\hat{\boldsymbol{y}}. \tag{2.50}$$

Here L_1 is the circumference in the x-direction and L_2 is the circumference in the y-direction. The vector potential $\boldsymbol{A}$ corresponds to the component of the magnetic field perpendicular to the carbon nanotube.

To describe the system quantum mechanically, the following two options are equivalent:

1. A Hamiltonian that is a function of only $\boldsymbol{A}$ and not $\boldsymbol{A}_{total}$. In this case we incorporate $\theta h/e$ and $\phi h/e$ in the boundary conditions that are imposed on the wavefunctions.

2. A Hamiltonian that is a function of $\boldsymbol{A}_{total}$. In this case the boundary conditions are independent of θ and ϕ.

We use the second option to derive an expression of the Hall conductance in terms of the partial derivatives of the ground state wavefunction. However, it is important to take note of the

first option. It is the first option that allows us to argue that the conductance is independent of θ and ϕ when the Fermi energy is in a finite gap and the system is large enough. This enable us to rewrite the Hall conductance into an integral which reveals the topological nature of the Hall conductance.

The Kubo formula in terms of many-body eigenstates is given by:

$$\sigma_{yx} = \frac{\imath e^2 \hbar}{A} \sum_{n>0} \frac{\langle 0 | v_y | n \rangle \langle n | v_x | 0 \rangle - \langle 0 | v_x | n \rangle \langle n | v_y | 0 \rangle}{(E_n - E_0)^2}. \tag{2.51}$$

Here $A = L_1 L_2$ is the area of the system. The eigenenergies E_0 and E_n correspond to the many-body ground state $|0\rangle$ and the excited states $|n\rangle$ of the system. The sum is over all the excited states. The fundamental definition of the velocity operators that appear in the Kubo formula are (we explain these expressions in section 2.3):

$$\begin{aligned} v_x &= \frac{L_1}{\hbar} \frac{\partial H}{\partial \theta}, \\ v_y &= \frac{L_2}{\hbar} \frac{\partial H}{\partial \phi}. \end{aligned} \tag{2.52}$$

In terms of $\partial_\phi H$ and $\partial_\theta H$, Equation (2.51) becomes

$$\sigma_{yx} = \frac{\imath e^2}{\hbar} \sum_{n>0} \frac{\langle 0 | \partial_\phi H | n \rangle \langle n | \partial_\theta H | 0 \rangle - \langle 0 | \partial_\theta H | n \rangle \langle n | \partial_\phi H | 0 \rangle}{(E_n - E_0)^2}. \tag{2.53}$$

Owing to the fact that $|n\rangle$ is orthogonal to $|0\rangle$, we have

$$\begin{aligned} 0 &= E_n \langle 0 | n \rangle = \langle 0 | H | n \rangle \\ &\Rightarrow \partial_\phi \langle 0 | H | n \rangle = 0. \end{aligned} \tag{2.54}$$

Since:

$$\partial_\phi \langle 0 | H | n \rangle = [\partial_\phi \langle 0 |] | H | n \rangle + \langle 0 | \partial_\phi H | n \rangle + \langle 0 | H \partial_\phi | n \rangle, \tag{2.55}$$

it follows that

$$\langle 0 | \partial_\phi H | n \rangle = -E_n [\partial_\phi \langle 0 |] | n \rangle - E_0 \langle 0 | \partial_\phi | n \rangle. \tag{2.56}$$

Because $|0\rangle$ is orthogonal to $|n\rangle$,

$$
\begin{aligned}
0 = \partial_\phi \langle 0|n\rangle &= [\partial_\phi \langle 0|] |n\rangle + \langle 0| \partial_\phi |n\rangle \\
\Rightarrow \langle 0| \partial_\phi |n\rangle &= - [\partial_\phi \langle 0|] |n\rangle .
\end{aligned}
\tag{2.57}
$$

Substituting this into Equation (2.56) we find that

$$
\langle 0| \partial_\phi H |n\rangle = (E_0 - E_n) [\partial_\phi \langle 0|] |n\rangle .
\tag{2.58}
$$

Similarly, the other term in the Kubo formula that contains $\partial_\phi H$ can be calculated and is given by

$$
\langle n| \partial_\phi H |0\rangle = (E_0 - E_n) \langle n| \partial_\phi |0\rangle .
\tag{2.59}
$$

We derive $\langle 0| \partial_\theta H |n\rangle$ and $\langle n| \partial_\theta H |0\rangle$ in the same way:

$$
\langle 0| \partial_\theta H |n\rangle = (E_0 - E_n) [\partial_\theta \langle 0|] |n\rangle ,
\tag{2.60a}
$$

$$
\langle n| \partial_\theta H |0\rangle = (E_0 - E_n) \langle n| \partial_\theta |0\rangle .
\tag{2.60b}
$$

Substitute Equation (2.58), Equation (2.59), Equation (2.60a) and Equation (2.60b) back into Equation (2.51), the Hall conductance is now given by:

$$
\sigma_{yx} = \frac{\imath e^2}{\hbar} \sum_{n>0} [\partial_\phi \langle 0|] |n\rangle \langle n| \partial_\theta |0\rangle - [\partial_\theta \langle 0|] |n\rangle \langle n| \partial_\phi |0\rangle .
\tag{2.61}
$$

We can incorporate the term $n = 0$ into the sum, because it is zero. From the fact that $|n\rangle$ is a complete basis follows:

$$
\sum_n |n\rangle \langle n| = \mathbb{I}.
\tag{2.62}
$$

We are now able to express Equation (2.51) in terms of the partial derivatives of the ground state wavefunction of the many-body system:

$$
\sigma_{yx} = \frac{\imath e^2}{\hbar} [\partial_\phi \langle 0|] \partial_\theta |0\rangle - [\partial_\theta \langle 0|] \partial_\phi |0\rangle .
\tag{2.63}
$$

At this point it is still not clear why the Hall conductance should be quantized. To show the quantization, we need to assume that there is a finite gap between the ground state and the excited states. We explained earlier that the effect of the magnetic flux can be incorporated in

the boundary condition. In this circumstance, Nui et al. argued it is plausible that the effect on the bulk should be insensitive to the boundary conditions and are therefore independent of the parameters θ and ϕ. If this is the case, we can compute σ_{yx} for different boundary conditions and take the average over all the phases ($0 \leq \theta < 2\pi, 0 < \phi \leq 2\pi$):

$$\sigma_{yx} = \bar{\sigma}_{yx} = \frac{\imath e^2}{h} \int_0^{2\pi} \int_0^{2\pi} d\theta \, d\phi \frac{1}{2\pi} \left([\partial_\phi \langle 0|] \, \partial_\theta \, |0\rangle - [\partial_\theta \langle 0|] \, \partial_\phi \, |0\rangle \right). \tag{2.64}$$

We must emphasize here that in the nanotube system it is not allowed to replace σ_{yx} with $\bar{\sigma}_{yx}$, because of the smallness of realistic tube radii. Statements made below regarding σ_{yx} therefore are replaced with corresponding statements regarding the averaged quantity $\bar{\sigma}_{yx}$ only, when the argument is applied to the nanotube system.

To show that the Hall conductance is quantized into an integer times e^2/h when the phase parameters, θ or ϕ changes with 2π, we define

$$\boldsymbol{\mathcal{A}} \;=\; \mathcal{A}_\theta \hat{\theta} + \mathcal{A}_\phi \hat{\phi}, \tag{2.65}$$

where $\mathcal{A}_\theta = \langle 0| \, \partial_\theta \, |0\rangle$ and $\mathcal{A}_\phi = \langle 0| \, \partial_\phi \, |0\rangle$. We also define the following vector derivative:

$$\boldsymbol{\partial} = \partial_\theta \hat{\theta} + \partial_\phi \hat{\phi}. \tag{2.66}$$

In terms of Equation (2.65) and Equation (2.66), Equation (2.64) can be rewritten as follows:

$$\sigma_{yx} = \frac{\imath e^2}{h} \int_S \frac{d\boldsymbol{a}}{2\pi} \cdot \boldsymbol{\partial} \times \boldsymbol{\mathcal{A}}. \tag{2.67}$$

Here $d\boldsymbol{a}$ is an infinitesimal area element that is perpendicular to the $\theta - \phi$ plane. Stokes' theorem allows us to rewrite the surface integral of the curl of the vector field in terms of a line integral of the vector field and Equation (2.67) becomes:

$$
\begin{aligned}
\sigma_{yx} &= \frac{\imath e^2}{h} \frac{1}{2\pi} \oint_{\partial S} d\boldsymbol{l} \cdot \boldsymbol{\mathcal{A}} \\
&= \frac{\imath e^2}{h} \frac{1}{2\pi} \left\{ \int_0^{2\pi} d\phi \left[\mathcal{A}_\phi \left(\phi, 0 \right) - \mathcal{A}_\phi \left(\phi, 2\pi \right) \right] + \int_0^{2\pi} d\theta \left[\mathcal{A}_\theta \left(2\pi, \theta \right) - \mathcal{A}_\phi \left(0, \theta \right) \right] \right\}.
\end{aligned}
\tag{2.68}
$$

We assume that there is always a finite gap between the ground state and the excited state when θ and ϕ varies from 0 to 2π, that is to say, if we vary the flux by one flux quantum. Under these

circumstances, a fundamental result of quantum mechanics dictates that the ground state will to return back to itself up to a phase factor:

$$|0\rangle_{\phi,2\pi} = e^{\imath f(\phi)} |0\rangle_{(\phi,0)}, \tag{2.69a}$$

$$|0\rangle_{2\pi,\theta} = e^{\imath g(\theta)} |0\rangle_{(0,\theta)}. \tag{2.69b}$$

There exists a connection between the phases f and g: Consider the ground state at $(\phi, \theta) = (2\pi, 2\pi)$. If we firstly use Equation (2.69a) and then Equation (2.69b), we find:

$$\begin{aligned}
|0\rangle_{2\pi,2\pi} &= e^{\imath f(2\pi)} |0\rangle_{(2\pi,0)}, \\
&= e^{\imath f(2\pi)+\imath g(0)} |0\rangle_{(0,0)}.
\end{aligned} \tag{2.70}$$

But if we firstly use Equation (2.69b) and then Equation (2.69a), we find:

$$\begin{aligned}
|0\rangle_{2\pi,2\pi} &= e^{\imath g(2\pi)} |0\rangle_{(0,2\pi)}, \\
&= e^{\imath g(2\pi)+\imath f(0)} |0\rangle_{(0,0)}.
\end{aligned} \tag{2.71}$$

Together Equation (2.70) and Equation (2.71) implies

$$f(2\pi) - f(0) + g(0) - g(2\pi) = 2\pi n, \tag{2.72}$$

with $n \in \mathbb{Z}$. Furthermore, from Equation (2.69a) follows:

$$\begin{aligned}
\mathcal{A}_\phi(\phi, 2\pi) &= \langle 0| e^{-\imath f(\phi)} \partial_\phi e^{\imath f(\phi)} |0\rangle_{(\phi,0)}, \\
&= \imath \partial_\phi f(\phi) + \mathcal{A}_\phi(\phi, 0),
\end{aligned} \tag{2.73}$$

And from Equation (2.69b) follows:

$$\begin{aligned}
\mathcal{A}_\theta(2\pi, \theta) &= \langle 0| e^{-\imath g(\theta)} \partial_\phi e^{\imath g(\theta)} |0\rangle_{(0,\theta)}, \\
&= \imath \partial_\theta g(\theta) + \mathcal{A}_\theta(0, \theta).
\end{aligned} \tag{2.74}$$

By substituting Equation (2.73) and Equation (2.74) into Equation (2.68) and making use of

Equation (2.72), we find the Hall conductance to be an integer multiple of e^2/h:

$$
\begin{aligned}
\sigma_{yx} &= \frac{\imath e^2}{h} \times \frac{1}{2\pi} \left\{ \int_0^{2\pi} d\phi \, (-\imath \partial_\phi f(\phi)) + \int_0^{2\pi} d\theta \, (\imath \partial_\theta g(\theta)) \right\} \\
&= \frac{e^2}{h} \times \frac{1}{2\pi} \left\{ f(2\pi) - f(0) + g(0) - g(2\pi) \right\} \\
&= n \frac{e^2}{h}.
\end{aligned}
\tag{2.75}
$$

Here $n = 0$ is a possibility.

2.3   Derivation of the velocity operators

Here we derive the expressions that is used for the velocity operators in our derivation of the quantization of the Hall conductance.

A single particle in a classical system is described by the Hamiltonian $H(\boldsymbol{p}, \boldsymbol{x})$. According to Hamilton's equations, the velocity of the particle is:

$$
\frac{d\boldsymbol{x}}{dt} = \frac{\partial H}{\partial \boldsymbol{p}}.
\tag{2.76}
$$

In a quantum mechanical description of the system, $\boldsymbol{x}$, $\boldsymbol{p}$ and H are operators and Equation (2.76) does not make any sense, because a derivative with respect to an operator is not a well defined operation. One can get around this problem by realizing the classical vector potential ($\boldsymbol{A}$) in the Hamiltonian formalism always appears in the following combination:

$$
\boldsymbol{p} + e\boldsymbol{A}_{total}.
\tag{2.77}
$$

We choose the total vector potential to be equal to:

$$
\boldsymbol{A}_{total} = \boldsymbol{A} + \boldsymbol{\alpha}.
\tag{2.78}
$$

Here $\boldsymbol{A}$ includes the effect of any magnetic field and $\boldsymbol{\alpha} = \alpha_x \hat{x} + \alpha_y \hat{y}$ is constant in space. Due to Equation (2.77), classically we can write the following:

$$
\frac{\partial H}{\partial \boldsymbol{p}} = \frac{1}{e} \frac{\partial H}{\partial \boldsymbol{\alpha}}.
\tag{2.79}
$$

On the quantum level, we therefore define the velocity operator as follows:

$$\boldsymbol{v} \equiv \frac{1}{e}\frac{\partial H}{\partial \boldsymbol{\alpha}}. \tag{2.80}$$

This is also valid for tight binding systems in which particles are allowed to occur only at a discrete collection of positions. For a general tight binding Hamiltonian

$$H = \sum_{nm} t^{nm} |\boldsymbol{x}_n\rangle \langle \boldsymbol{x}_m|, \tag{2.81}$$

the constant contribution to the vector potential, $\boldsymbol{\alpha}$, is represented by a phase:

$$t^{nm} = t e^{-\imath \frac{e}{\hbar}\boldsymbol{\alpha}\cdot(\boldsymbol{x}_n - \boldsymbol{x}_m)}. \tag{2.82}$$

This leads to the following general result for a velocity operator:

$$\boldsymbol{v} = -\frac{\imath}{\hbar}\sum_{nm} t^{nm}(\boldsymbol{x}_n - \boldsymbol{x}_m)|\boldsymbol{x}_n\rangle\langle \boldsymbol{x}_m| \tag{2.83}$$

For the graphene Hamiltonian, Equation (2.5), we have:

$$
\begin{aligned}
\boldsymbol{v} = {} & \frac{\imath}{\hbar}\sum_{nm} t_0^{mn}\boldsymbol{d}_0 |m,n,B\rangle\langle m,n,A| \\
& + \frac{\imath}{\hbar}\sum_{nm} t_1^{mn}\boldsymbol{d}_1 |m+1,n,B\rangle\langle m,n,A| \\
& + \frac{\imath}{\hbar}\sum_{nm} t_2^{mn}\boldsymbol{d}_2 |m,n+1,B\rangle\langle m,n,A| - h.c.
\end{aligned} \tag{2.84}
$$

The minus sign of Equation (2.83) cancel out, because by definition $\boldsymbol{d}_j$, (j = 0,1,2) connects a B-type atom with a A-type atom, whereas the terms in Equation (2.84) represents hopping from a A-type atom to a B-type atom.

The components of $\boldsymbol{v}$ are obtained by breaking up $\boldsymbol{d}$ in its x and y components. The x and y components of $\boldsymbol{v}$ are therefore found to be:

$$v_x = \frac{\imath a}{2\hbar}\left[\sum_{nm} t_1^{nm}|m+1,n,B\rangle\langle m,n,A| - t_2^{nm}|m,n+1,B\rangle\langle m,n,A| - h.c.\right], \tag{2.85}$$

$$v_y = \frac{\imath a}{2\sqrt{3}\hbar} \left[\sum_{nm} t_1^{nm} |m+1, n, B\rangle \langle m, n, A| + t_2^{nm} |m, n+1, B\rangle \langle m, n, A| \right]$$
$$- \frac{\imath a}{2\sqrt{3}\hbar} \left[\sum_{nm} 2 t_0^{mn} |m, n, B\rangle \langle m, n, A| + h.c. \right]. \tag{2.86}$$

2.4 Kubo formula in terms of single particle states

Thus far we discussed the Kubo formula in terms of many-body eigenstates and energies of the system. If there is no interaction present, the many-body eigenstates are just anti-symmetrized products of single particle states and the many-body energies are the sum of single particle energies. It is therefore possible to rewrite Equation (2.51) in terms of single particle states and single particle energies. Equation (2.51) is the most convenient form to reveal the topological quantization of the Hall conductance, but the single particle formula is more convenient for the calculations that we shall present in later chapters. For this reason, we derive the single particle formula.

Consider a non-interacting system with single particle eigenstates $|\alpha\rangle$ and single particle energies ϵ_α. The associated fermion creation and annihilation operators are $C_\alpha^\dagger$ and C_α. The ground state is represented as

$$|0\rangle = \prod_{\alpha < E_F} C_\alpha^\dagger |\text{vac}\rangle, \tag{2.87}$$

with energy

$$E_0 = \sum_{\epsilon_\alpha < E_F} \epsilon_\alpha, \tag{2.88}$$

The state, $|\text{vac}\rangle$, represents the vacuum and E_F the Fermi energy. The velocity operators v_x and v_y are:

$$v_q = \sum_{\alpha\beta} \langle \alpha | v_q^{(1)} | \beta \rangle C_\alpha^\dagger C_\beta, \tag{2.89}$$

where $v_q^{(1)}$ refer to the single particle velocity operators defined in the previous section. We notice that v_q removes one particle with the operator C_β and create a particle with $C_\alpha^\dagger$. The state $v_q |0\rangle$ contains therefore only one particle - hole pair and the matrix elements $\langle n| v_q |0\rangle$ and $\langle 0| v_{q'} |n\rangle$ are equal to zero, unless $|n\rangle$ is an excited state that contains only one particle - hole pair. We can therefore limit the sum in Equation (2.51) to the excited state of the form:

$$|n\rangle = C_\mu^\dagger C_\upsilon |0\rangle. \tag{2.90}$$

Here $\epsilon_\mu > E_F$ and $\epsilon_\upsilon < E_F$. Such a state has an energy $E_n = \epsilon_\mu - \epsilon_\upsilon + E_0$ and therefore we can write $E_n - E_0 = \epsilon_\mu - \epsilon_\upsilon$.

From Equation (2.89) and Equation (2.90), the matrix element $\langle 0|\, v_q\, |n\rangle$ is given by:

$$\langle 0|\, v_q\, |n\rangle = \sum_{\alpha\beta} \langle\alpha|\, v_q^{(1)}\, |\beta\rangle \, \langle 0|\, C_\alpha^\dagger C_\beta C_\mu^\dagger C_\upsilon\, |0\rangle . \tag{2.91}$$

From Wick's theorem follows:

$$\langle 0|\, C_\alpha^\dagger C_\beta C_\mu^\dagger C_\upsilon\, |0\rangle = \langle 0|\, C_\alpha^\dagger C_\beta\, |0\rangle \, \langle 0|\, C_\mu^\dagger C_\upsilon\, |0\rangle + \langle 0|\, C_\alpha^\dagger C_\upsilon\, |0\rangle \, \langle 0|\, C_\beta C_\upsilon^\dagger\, |0\rangle . \tag{2.92}$$

The first term on the right hand side of Equation (2.92) is equal to zero because υ refer to a state with an energy $\epsilon_\upsilon < E_F$, while μ refer to a state with energy $\epsilon_\mu > E_F$. Therefore, μ is unequal to υ and the state $C_\nu^\dagger C_\upsilon\, |0\rangle$ contains a particle - hole excitation while $|0\rangle$ does not contain a particle - hole excitation.

The second term on the right hand side is equal to one if and only if $\alpha = \upsilon$, $\epsilon_\alpha < E_F$, $\beta = \mu$ and $\epsilon_\beta > E_F$. If we substitute this into Equation (2.51), we obtain the single particle formula for the Kubo formula:

$$\sigma_{yx} = \frac{\imath e^2 \hbar}{A} \sum_{\epsilon_\alpha < E_F < \epsilon_\beta} \frac{\langle\alpha|\, v_y^{(1)}\, |\beta\rangle \, \langle\beta|\, v_x^{(1)}\, |\alpha\rangle - \langle\alpha|\, v_x^{(1)}\, |\beta\rangle \, \langle\beta|\, v_y^{(1)}\, |\alpha\rangle}{(\epsilon_\alpha - \epsilon_\beta)^2} \tag{2.93}$$

where $|\alpha\rangle$ and $|\beta\rangle$ are single particle eigenstates.

CHAPTER 3
Analytical calculations

In the rest of this thesis we study a quantum Hall effect that occurs in carbon nanotubes. This effect can be observed when an external magnetic field, $\boldsymbol{B}$, and electric field, $\boldsymbol{E}$, are applied parallel to each other and perpendicular to the tube-axis. Furthermore, a flux ,Φ, is assumed to thread the tube. When this flux is varied, it produces an electromotive force (emf) around the circumference of the tube. We shall show that this produces a quantized Hall current along the axis of the tube.

The mechanism behind this effect is: Firstly the electrostatic potential, that is either correlated or anti-correlated with the magnetic field, induces a gap between the valence band and the conduction band of a previously metallic carbon nanotube [14]. Secondly, the electronic wave-functions are modified as follows. Let $\boldsymbol{B}_{\perp}$ be the component of the magnetic field that is perpendicular to the surface of the sample. If the magnetic field and electric field are correlated i.e.

$$\int_{Area} dx \, dy \, \boldsymbol{B}_{\perp}(x,y)U(x,y) > 0, \tag{3.1}$$

then the highest valence band electron states is localized in regions where $\boldsymbol{B}_{\perp} < 0$. Contrary to this, when the magnetic field and electric field are anti-correlated i.e.

$$\int_{Area} dx \, dy \, \boldsymbol{B}_{\perp}(x,y)U(x,y) < 0, \tag{3.2}$$

the highest valence band electron states is localized in regions where $\boldsymbol{B}_{\perp} > 0$. Either way, the lowest conduction band electron states are localized in regions where the sign of $\boldsymbol{B}_{\perp}$ is the opposite as indicated above. In a low temperature sample only the states in the valence band are occupied. Therefore, the occupied electronic orbitals experience a magnetic field that does not average to zero. It is therefore plausible that the electrons in these orbitals all experience a Lorentz force in the same direction, when an electric field establishes a current. Based on this argument, a non-zero Hall effect is expected.

In order to observe the Hall effect that we investigate, the flux, Φ, threading the tube must be varied an amount of the order of one flux quantum, $\phi = e/h$. Since realistic values for the
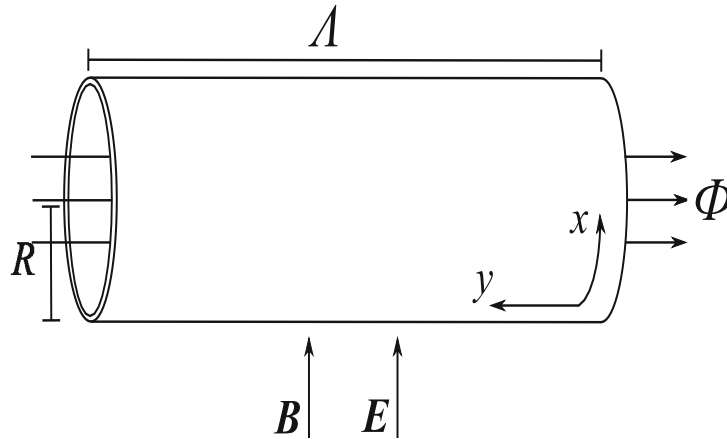
33

Figure 3.1: **A carbon nanotube in the presence of a constant magnetic field B and electric field E, parallel to each other and perpendicular to the tube axis. An additional magnetic field is applied parallel to the cylinder axis, in such a way that a magnetic flux Φ threads the tube. The length of the tube Λ, is much bigger than the radius R. The y-axis is chosen to point in the direction of the tube axis and the x-axis is chosen to be along the circumference.**

magnetic field are ~ 30 Tesla at the most, there is a restriction on the minimum allowed tube radius. At 30 Tesla the flux Φ would be greater than e/h when the tube radius R is larger than seven nanometer. However, single wall carbon nanotubes have radii smaller than three nanometer. We propose two possible ways around this problem:

1. A multi-wall carbon nanotube, consisting out of multiple carbon nanotubes within each other, have outer-radii of several tens of nanometers. Several experimental studies have shown that for multi-wall carbon nanotubes subjected to suitable conditions, such as low temperatures and small bias voltages, the electron transport is restricted to the outermost wall [26], [27], [28]. Therefore it seems plausible that the effect we investigate here can also be observed in multi-wall tubes.

2. A method to fabricate large-radius single wall tubes exists [29], [30]. The idea is to manually remove the inner cylinders of a multi-wall carbon nanotube until only the outer cylinder remains. As far as we are aware, this method has not yet been applied to remove all but the outermost cylinder, but we see no fundamental obstacles in doing so.

In the remaining part of this chapter we present analytical calculations for this system. As we point out below, the analytical calculations involves certain approximations. In Chapter 3 we obtain numerical results to confirm the validity of these approximations.

Firstly, we shall investigate whether a magnetic field and electric field, parallel to each other and perpendicular to the tube-axis, induce a gap between the valence band and the conduction band in a carbon nanotube. We shall present both exact and perturbation results which reveal that a gap is induced. Having established the existence of a gapped state, we shall proceed to investigate whether the gapped state supports a Hall effect as we suspected. To do so, we calculate the Hall conductance in the regime where the magnetic field is large compared to the applied electric field ($v_F \boldsymbol{B} > \boldsymbol{E}$).

3.1 The system

As shown in Figure 3, we choose $\hat{\boldsymbol{x}}$ to be along the circumference, $\hat{\boldsymbol{y}}$ to point along the tube axis while $\hat{\boldsymbol{z}}$ is the direction perpendicular to the wall of the tube. Because electrons are confined to the tube wall, the effective magnetic field is in the $\hat{\boldsymbol{z}}$ direction:

$$\boldsymbol{B} = B(x)(\hat{\boldsymbol{z}}). \tag{3.3a}$$

The electrostatic potential is given by

$$U = U(x). \tag{3.3b}$$

The magnetic field and electric field obey the following boundary conditions:

$$\boldsymbol{B}(x + L) = \boldsymbol{B}(x), \tag{3.4a}$$

$$U(x + L) = U(x), \tag{3.4b}$$

where $L = 2\pi R$ is the tube circumference.

In a realistic experiment, the magnetic field and the electric field will be constant on the scale of the radius of the tube. When the tube is exposed to a constant magnetic field and electric field perpendicular to the axis of the tube, electrons in the tube wall see sinusoidal magnetic field and electrostatic potential:

$$\boldsymbol{B} = B_0 \cos\left(\frac{2\pi}{L}x\right)\hat{\boldsymbol{z}}, \tag{3.5a}$$

$$U = -U_0 \cos\left(\frac{2\pi}{L}x\right). \tag{3.5b}$$
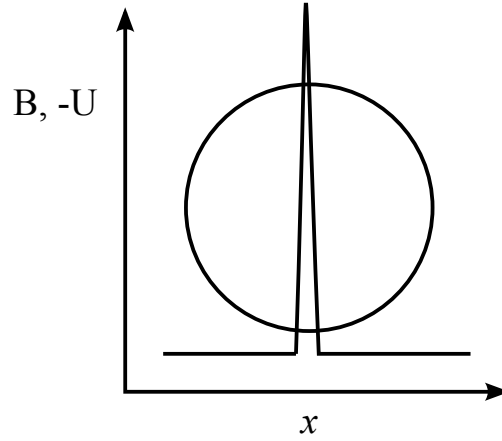
Figure 3.2: Representation of the δ-function magnetic field that is applied to the carbon nanotube.

The corresponding vector potential $(\boldsymbol{B} = \boldsymbol{\partial_r} \times \boldsymbol{A})$ is

$$\boldsymbol{A} \;\; = \;\; B_0 \frac{2\pi}{L} \sin\left(\frac{2\pi}{L}x\right) \boldsymbol{\hat{y}}. \tag{3.6}$$

This situation will be investigated later on. We will calculate the spectrum with perturbation theory close to the Dirac point in the regime where $\upsilon_F \boldsymbol{B} > \boldsymbol{E}$, but firstly we review a toy model for which exact results for the energy spectrum has been obtained [14], [32] and [33]. This model is less realistic than the situation described above, but confirms that the electrons localize in maxima and minima of the magnetic field and that a gapped state is induced. The magnetic field and electrostatic potential for this model are taken as

$$\boldsymbol{B} \;\; = \;\; B_0 L \left[\delta(x) - \delta\left(x - \frac{L}{2} \right) \right] \boldsymbol{\hat{z}}, \tag{3.7a}$$

$$U \;\; = \;\; -U_0 L \left[\delta(x) - \delta\left(x - \frac{L}{2} \right) \right]. \tag{3.7b}$$

The corresponding vector potential is a step function given by

$$\boldsymbol{A} = B_0 L \left[\theta(x) - \theta\left(x - \frac{L}{2} \right) \right] \boldsymbol{\hat{y}}. \tag{3.8}$$

The representation of the magnetic field, scalar potential and vector potential along the circumference are illustrated in Figure 3.2 and Figure 3.3.

In the following section the spectrum of this model is calculated. We shall only consider
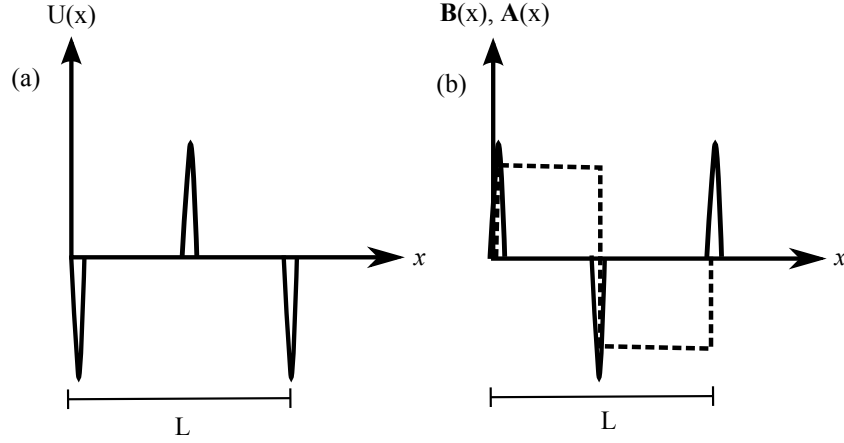
Figure 3.3: (a) **A schematic diagram of the δ-function scalar potential seen by electrons in the tube wall. (b) The solid line represents the one dimensional δ-function magnetic field and the dotted line the corresponding vector potential on the circumference of the tube.**

carbon nanotubes which were metallic before the magnetic and electric fields were switched on. The reasoning behind this is that we want to study gap-formation, thus we shall work with tubes that are gapless when $\boldsymbol{B}$ and U are zero.

3.2 Gapped state in δ-function magnetic and electric fields

When we consider the toy model described above and the scalar potential U is set to zero, we find that the Dirac equation $H\psi = E\psi$ has two zero energy states $\psi_\pm$, with

$$\psi_{0,+}(x) \propto \begin{pmatrix} e^{F(x)} \\ 0 \end{pmatrix}, \tag{3.9a}$$

$$\psi_{0,-}(x) \propto \begin{pmatrix} 0 \\ e^{-F(x)} \end{pmatrix}, \tag{3.9b}$$

where

$$F(x) = \sqrt{eLB_0}\left|x - \frac{L}{2}\right|. \tag{3.10}$$

The state ψ_- has its maximum at $x = 0$, where $\boldsymbol{B}_\perp$ is maximal and falls of exponentially away from the maximum. Similarly, the state ψ_+ has its maximum where $\boldsymbol{B}_\perp$ is minimum. We now show that by adding an electric field to the toy model, a gap is induced in the spectrum.

To calculate the spectrum of this system, we choose the units such that $\hbar$ and the Fermi velocity, v_F, in the Dirac equation equals one. The Dirac equation for an eigenstate, Ψ, with energy, E, reads

$$\{\sigma_y \cdot [-\imath\partial_y + eA(x)] + \sigma_x \cdot (-\imath\partial_x) + U(x)\}\Psi = E\Psi. \tag{3.11}$$

Because of translation invariance in the y-direction, $\Psi(x,y)$ factorizes as $\Psi = e^{\imath ky}\psi(x)$. The wave function, $\psi(x)$, satisfies

$$\{\sigma_y \cdot [k + eA(x)] + \sigma_x \cdot (-\imath\partial_x) + U(x)\}\psi = E\psi. \tag{3.12}$$

We multiply Equation (3.12) with $\imath\sigma_x$ and rearrange the terms to find

$$\partial_x\psi(x) \quad = \quad M(x)\psi(x), \tag{3.13}$$

where

$$M(x) = \imath\sigma_x[E - U(x)] - \sigma_z \cdot [k + eA(x)]. \tag{3.14}$$

The solution of the matrix differential equation, Equation (3.13) is given by

$$\psi(x) = \mathcal{X}\exp\int_0^x dx' M(x)\psi(0), \tag{3.15}$$

where $\mathcal{X}\exp$ is a position ordered exponent with the largest argument to the left.

We now define

$$T(x) = \mathcal{X}\exp\int_0^x dx' M(x). \tag{3.16}$$

and divide the interval $[0,x]$ into four intervals $I_1 = [-\epsilon, \epsilon]$, $I_2 = \left[\epsilon, \frac{L}{2} - \epsilon\right]$, $I_3 = \left[\frac{L}{2} - \epsilon, \frac{L}{2} + \epsilon\right]$ and $I_4 = \left[\frac{L}{2} + \epsilon, L - \epsilon\right]$. Here ϵ is an infinitesimal positive number. M is constant in the intervals I_2 and I_4 while in the intervals I_1 and I_3 only the δ-function contribution survives. We can therefore write $T(L)$ as

$$T(L) = e^{M_4}e^{M_3}e^{M_2}e^{M_1}, \tag{3.17}$$

where

$$M_i = \int_{I_i} dx\, M\left(x\right), \tag{3.18}$$

for $i = 1, 2, 3$ and 4. Explicitly the four matrices are

$$M_1 = \begin{pmatrix} 0 & U_0 \\ -U_0 & 0 \end{pmatrix} L, \tag{3.19a}$$

$$M_2 = \begin{pmatrix} -k - \frac{1}{2}eB_0L & E \\ -E & k + \frac{1}{2}eB_0L \end{pmatrix} \frac{L}{2}, \tag{3.19b}$$

$$M_3 = \begin{pmatrix} 0 & -U_0 \\ U_0 & 0 \end{pmatrix} L, \tag{3.19c}$$

$$M_4 = \begin{pmatrix} -k + \frac{1}{2}eB_0L & E \\ -E & k - \frac{1}{2}eB_0L \end{pmatrix} \frac{L}{2}. \tag{3.19d}$$

We are now in the position to compute the power series given by

$$e^A = \sum_{n=0}^{\infty} \frac{1}{n!} A^n, \tag{3.20}$$

for each of the matrices above. It is worth noticing that the four matrices M_1, M_2, M_3 and M_4 each has the property that its square is proportional to the identity matrix $\mathbb{I}$. Using this property the power series simplifies as follows

$$
\begin{aligned}
e^{M_i} &= \sum_{n=0}^{\infty} \frac{1}{n!} M_i^n \\
&= \sum_{n=0}^{\infty} \left(\frac{M_i^{2n}}{(2n)!} + \frac{M_i^{2n+1}}{(2n+1)!} \right) \\
&= \sum_{n=0}^{\infty} \left(\frac{c_i^{2n}}{(2n)!} + M_i \frac{c_i^{2n}}{(2n+1)!} \right) \\
&= \sum_{n=0}^{\infty} \left(\frac{c_i^{2n}}{(2n)!} + \frac{1}{c_i} M_i \frac{c_i^{2n+1}}{(2n+1)!} \right) \\
&= \cosh\left(c_i\right) + \frac{1}{c_i} M_i \sinh\left(c_i\right),
\end{aligned}
\tag{3.21}
$$

where $M_i^2 = \mathbb{I}c_i^2$ for $i = 1, 2, 3$ and 4. We now calculate the value of the constant c for each of

the different matrices M_1, M_2, M_3 and M_4.

$$M_1^2 = \begin{pmatrix} -U_0^2 & 0 \\ 0 & -U_0^2 \end{pmatrix} L^2 \tag{3.22}$$

$$= -U_0^2 L^2 \mathbb{I}$$

$$\therefore c_1 = \imath |U_0| L. \tag{3.23}$$

A similar calculation yields

$$c_3 = \imath |U_0| L \mathbb{I} \tag{3.24}$$

$$\therefore c_3 = c_1. \tag{3.25}$$

Let $k_\pm = k \pm \frac{1}{2} e B_0 L$, then

$$M_2^2 = \begin{pmatrix} k_+^2 - E^2 & 0 \\ 0 & k_+^2 - E^2 \end{pmatrix} \left(\frac{L}{2}\right)^2 \tag{3.26}$$

$$= [k_+^2 - E^2] \left(\frac{L}{2}\right)^2 \mathbb{I}$$

$$\therefore c_2 = \frac{L}{2} \sqrt{k_+^2 - E^2}. \tag{3.27}$$

The value of c_4, corresponding to the matrix M_4, is calculated in the same way as c_2 and is found to be

$$c_4 = \frac{L}{2} \sqrt{k_-^2 - E^2}. \tag{3.28}$$

Knowing the constant values c_1 and c_3, further simplification of e^{M_1} and e^{M_3} are possible,

$$
\begin{aligned}
e^{M_1} &= \cosh(c_1 L) + \frac{1}{c_1} M_1 \sinh(c_1 L) \\
&= \begin{pmatrix} \cosh(\imath |U_0| L) & \frac{U_0}{\imath |U_0|} \sinh(\imath |U_0| L) \\ -\frac{U_0}{\imath |U_0|} \sinh(\imath |U_0| L) & \cosh(\imath |U_0| L) \end{pmatrix} \\
&= \begin{pmatrix} \cos(U_0 L) & \frac{U_0}{|U_0|} \sin(|U_0| L) \\ -\frac{U_0}{|U_0|} \sin(|U_0| L) & \cos(U_0 L) \end{pmatrix} \\
&= \begin{pmatrix} \cos(U_0 L) & \mathrm{sgn}(U_0) \sin(|U_0| L) \\ -\mathrm{sgn}(U_0) \sin(|U_0| L) & \cos(U_0 L) \end{pmatrix} \\
&= \begin{pmatrix} \cos(U_0 L) & \sin(U_0 L) \\ -\sin(U_0 L) & \cos(U_0 L) \end{pmatrix}.
\end{aligned}
\tag{3.29}
$$

We can simplify e^{M_3} in the same way, so that

$$
\begin{aligned}
e^{M_3} &= \cosh(c_3 L) + \frac{1}{c_3} M_3 \sinh(c_3 L) \\
&= \begin{pmatrix} \cos(U_0 L) & -\sin(U_0 L) \\ \sin(U_0 L) & \cos(U_0 L) \end{pmatrix}.
\end{aligned}
\tag{3.30}
$$

$T(L)$ is a function of k and E, for given values of U_0, B_0 and L. We now calculate the dispersion relation for given values of U_0, B_0 and L. Enforcing the periodic boundary condition

$$
T(L)\Psi(0) = \Psi(0),
\tag{3.31}
$$

Equation (3.31) has the form of an eigenvalue equation which requires that $T(L)$ has an eigenvalue equal to one. We now use some of the general properties that $T(L)$ possesses to obtain an equivalent, but more convenient condition.

The determinant of $T(L)$ is equal to the product of its eigenvalues e_1 and e_2:

$$
\mathrm{Det}[T(L)] = e_1 e_2.
\tag{3.32}
$$

3. Analytical calculations 42

We calculate the determinant of $T(L)$ by using the fact that $\text{Det}(e^A) = e^{\text{tr}(A)}$.

$$
\begin{aligned}
\text{Det}[T(L)] &= \text{Det}[e^{M_4} e^{M_3} e^{M_2} e^{M_1}] \\
&= e^{\text{Tr}(M_4)} e^{\text{Tr}(M_3)} e^{\text{Tr}(M_2)} e^{\text{Tr}(M_1)} \\
&= e^0 e^0 e^0 e^0 \\
&= 1.
\end{aligned}
\tag{3.33}
$$

This implies that $e_1 e_2 = 1$, and therefore

$$
e_2 = \frac{1}{e_1}.
\tag{3.34}
$$

The trace of $T(L)$ is the sum of the eigenvalues and therefore

$$
\begin{aligned}
\text{Tr}[T(L)] \quad &= \quad e_1 + e_2 & \text{(3.35a)} \\
&= \quad e_1 + \frac{1}{e_1}. & \text{(3.35b)}
\end{aligned}
$$

Thus, if $T(L)$ has an eigenvalue $e_1 = 1$ then $\text{Tr}[T(L)] = 2$. The converse is also true, namely if $\text{Tr}[T(L)] = 2$ then $e_1 = 1$. To see this, we multiply Equation (3.35b) by e_1:

$$
\begin{aligned}
2e_1 &= e_1^2 + 1 \\
\Rightarrow (e_1 - 1)^2 &= 0 \\
\Rightarrow e_1 &= 1.
\end{aligned}
\tag{3.36}
$$

Equation (3.31) is therefore equivalent to the condition

$$
\text{Tr}\,[T(L)] = 2.
\tag{3.37}
$$

Using the explicit expressions for e^{M_i} where $i = 1, 2, 3$ and 4, Equation (3.37) becomes

$$
\begin{aligned}
0 = -1 + &\cosh\left(\frac{L}{2}\sqrt{k_+^2 - E^2}\right) \cosh\left(\frac{L}{2}\sqrt{k_-^2 - E^2}\right) + \frac{1}{\frac{L}{2}\sqrt{k_+^2 - E^2}\frac{L}{2}\sqrt{k_-^2 - E^2}} \\
&\times \sinh\left(\frac{L}{2}\sqrt{k_+^2 - E^2}\right) \sinh\left(\frac{L}{2}\sqrt{k_-^2 - E^2}\right) \left[k_+ k_- \cos\left(2U_0\right) - E^2\right].
\end{aligned}
\tag{3.38}
$$

3.2.1   Results

In Figure 3.4 the energy bands around the Dirac point are plotted as a function of k (the wave number in the y-direction) for different values of the magnetic field strength. Here the scalar
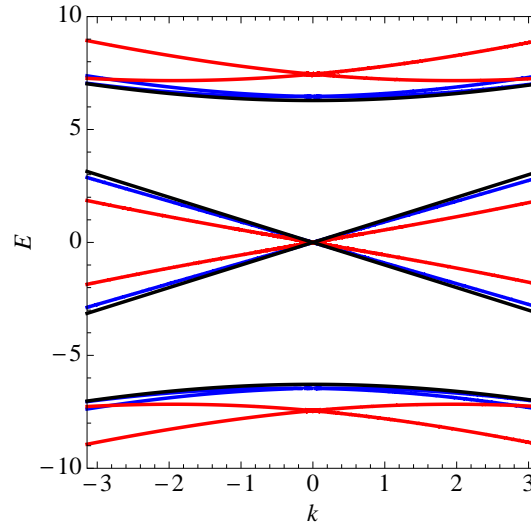
Figure 3.4: **Here we illustrate how the spectrum is modified for increasing values of the magnetic field, starting with zero magnetic field (black curve). We choose $B_0 = 3/eL$ in the blue curve and $B_0 = 8/eL$ in the red curve. The electrostatic potential U_0 is chosen to be zero.**

potential is equal to zero.

The effect of the magnetic field can be understood as follows. The black curve represents the situation where the magnetic field is absent, we choose $B_0 = \frac{3}{eL}$ for the blue curve and $B_0 = \frac{8}{eL}$ for the red curve. For increasing values of the magnetic field the dispersion relation flattens out, i.e. the Fermi velocity of the states around the Dirac points is reduced. This is reminiscent of the Landau levels that have zero dispersion in a 2D sample exposed to a constant magnetic field.

At zero magnetic field, the valence and conduction bands touch at $E = 0$ and are non-degenerate, while all the other bands are double degenerate. This degeneracy is due to time-reversal invariance. The degeneracy is therefore lifted when $\boldsymbol{B}$ is non-zero.

In Figure 3.5a we see that by applying an electrostatic potential U parallel to the magnetic field (blue curve), a gap is induced by decreasing the energy of ψ_+ and increasing the energy of ψ_-. States at the top of the valence band are all similar in character to ψ_+, in that they are predominantly peaked where $\boldsymbol{B}$ is negative. In a low temperature sample, only the valence band is occupied. In this case, since charge is concentrated around $y = 0$, most electrons in the sample effectively experience a negative magnetic field.

(a)   (b)
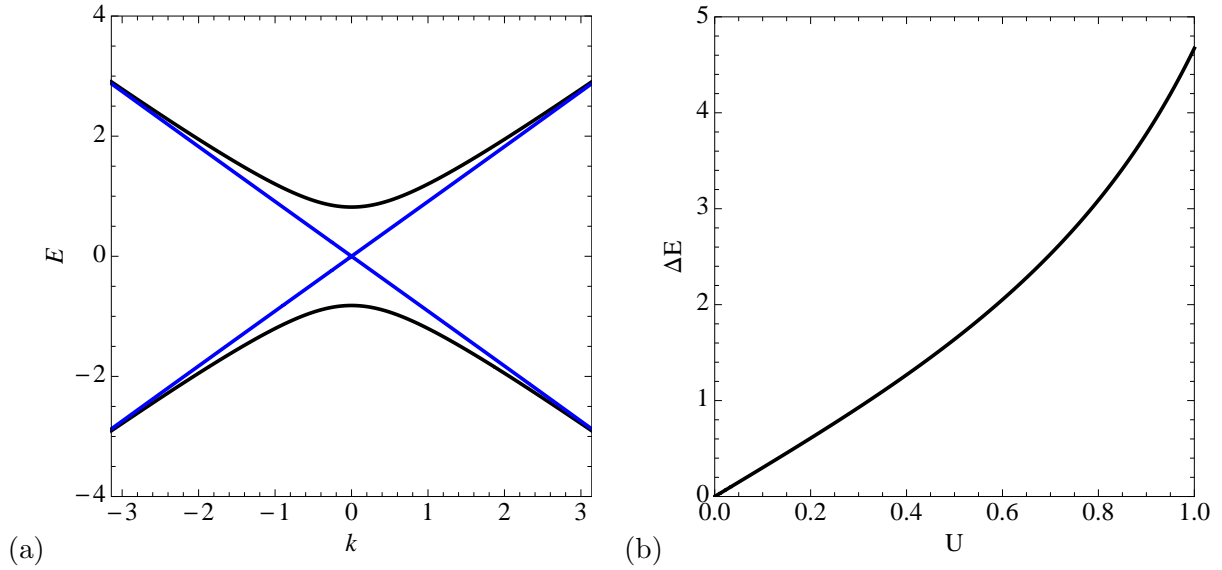
Figure 3.5: **(a) The band energy is plotted as a function of the wave vector k in the y-direction to show that the electric field induces a gap in the spectrum. In both situations the strength of the magnetic field is equal to $3/eL$. Firstly the blue curve represents the situations when the scalar potential is equal to zero. In the second situation, represented by the black curve, the scalar potential is chosen to be equal to $0.5/L$. (b) The size of the gap (ΔE) between the valence band and the conduction band is plotted as a function of the strength of the electrostatic potential.**

We now investigate the behavior of the gap ΔE as a function of the electrostatic potential U_0. The results are plotted in Figure 3.5b. The strength of the magnetic field is taken as B_0 = $\frac{3}{eL}$. From Figure 3.5 it is clear that the gap increases as the electrostatic potential increases. Therefore the size of the gap can be controlled by the electrostatic potential.

To conclude this section, we restate the main results: the toy model confirms that an electric field parallel to the magnetic field induces a gap in the spectrum of a previously metallic carbon nanotube. In a low temperature sample only the valence band is occupied and the states at the top of the valence band are predominantly peaked where the magnetic field is positive. The electric field biases these regions positively with respect to regions where conduction band electrons are localized. This opens up a gap between the valence and conduction bands.

The valence band electrons experience a negative magnetic field although the magnetic field averages to zero around the circumference of the tube. It is therefore relevant to investigate whether this gap supports a quantum Hall effect.

3.3 Gapped state in constant magnetic and electric fields perpendicular to the tube axis

The purpose of this study is to show that the gapped state that is induced with magnetic and electric fields that are parallel to each other and perpendicular to the tube axis, supports a quantum Hall effect. The Hall effect is studied by calculating the Hall conductance of the system when the Fermi energy is in the gap. In the previous section we obtained exact results that verified the existence of the gapped state, but the discussed situation is experimentally impractical. We shall investigate a more realistic experiment where the carbon nanotube experiences an electric field and a magnetic field as described by Equation (3.5a) and Equation (3.5b). The spectrum is calculated with perturbation theory, and the approximate expressions for the eigenstates and energies are substituted into the Kubo formula to calculate the Hall conductance.

The Kubo formula for the contribution of one valley τ to the Hall conductance is given by

$$
\sigma_{yx}^{\tau} = \frac{2e^2}{h} \frac{(\hbar v_F)^2}{\Lambda R} \int_0^L dx_1 \int_0^\Lambda dy_1 \int_0^L dx_2 \int_0^\Lambda dy_2 \sum_{\boldsymbol{k}_1, \boldsymbol{k}_2}
$$
$$
\frac{\mathrm{Im}\left\{ \left[\Psi_{\boldsymbol{k}_1-}(\boldsymbol{r}_1)^\dagger \sigma_y \Psi_{\boldsymbol{k}_2+}(\boldsymbol{r}_1) \right] \left[\Psi_{\boldsymbol{k}_2-}(\boldsymbol{r}_2)^\dagger \sigma_x \Psi_{\boldsymbol{k}_1+}(\boldsymbol{r}_2) \right] \right\}}{(\epsilon_1 - \epsilon_2)^2}, \tag{3.39}
$$

where $L = 2\pi R$ is the circumference of the tube, Λ is equal to the length of the tube, $v_F \sigma_x$ and $v_F \sigma_y$ are the velocity operators in the x and y direction respectively. The index $+$ refers to the positive energy solutions (conduction band), the index $-$ refers to the negative energy solutions (valence band) and τ distinguishes between the two valleys $\boldsymbol{K}$ and $\boldsymbol{K}'$. The index $\boldsymbol{k}$ is defined as $\boldsymbol{k} = k_x \hat{\mathbf{x}} + k_y \hat{\mathbf{y}}$, where

$$
k_x = \frac{m}{R} + \frac{\theta - 2\pi\nu\tau/3}{L}. \tag{3.40}
$$

Here m is an integer and represents the transverse modes, θ and ν are the same as defined in Chapter 2. The tube length Λ is assumed to be large enough that the results are independent of the boundary condition in the y-direction. For convenience we impose periodic boundary conditions along the length of the tube. Thus k_y is quantized in integer multiples of $2\pi/\Lambda$.

To calculate the Hall conductance we need to find the solutions for the wave functions $\Psi_{\boldsymbol{k}\pm}$, appearing in Equation (3.39). They are of the form

$$
\Psi_{\boldsymbol{k}\pm}(r) = e^{i\boldsymbol{k}\cdot\boldsymbol{r}} \psi_{\boldsymbol{k}\pm}(x)/\sqrt{\Lambda}. \tag{3.41}
$$

The wave function $\psi_{\boldsymbol{k}\pm}$ obeys periodic boundary conditions in the circumferential direction and satisfies $H(\boldsymbol{k})\psi_{\boldsymbol{k}\pm} = \epsilon_{\boldsymbol{k}\pm}\psi_{\boldsymbol{k}\pm}$; and $\epsilon_{\boldsymbol{k}\pm}$ are the energies of the eigenstates. The effective Hamiltonian $H(\boldsymbol{k})$ is given by $H(\boldsymbol{k}) = H_0 + H_1(\boldsymbol{k})$ with

$$H_0 \;=\; v_F\boldsymbol{\sigma}\cdot(-\imath\hbar\hat{\boldsymbol{x}}\partial_x + e\boldsymbol{A}), \tag{3.42a}$$

$$H_1(\boldsymbol{k}) \;=\; \hbar v_F\boldsymbol{\sigma}\cdot\boldsymbol{k} + U. \tag{3.42b}$$

To obtain the low-energy spectrum of $H(\boldsymbol{k})$, we first calculate the zero energy eigenstates of H_0. The zero energy eigenstates are found exactly. Using the zero energy eigenstates, $H_1(\boldsymbol{k})$ is then treated as a perturbation and approximate expressions for the eigenstates and energies are obtained. By substituting the approximate eigenstates and energies into the Kubo formula, the Hall conductance is derived analytically, as in [14].

3.3.1   Zero energy eigenstates

The aim is now to obtain the zero energy eigenstates of H_0. In the absence of the scalar potential U, the zero energy eigenstates of H_0 solve $H_0\psi_{\boldsymbol{k},\pm} = 0$. It can be easily shown that the two zero energy eigenstates are given by

$$\psi_{0,+} = N\begin{pmatrix} e^{F(x)} \\ 0 \end{pmatrix}, \tag{3.43a}$$

$$\psi_{0,-} = N\begin{pmatrix} 0 \\ e^{-F(x)} \end{pmatrix}, \tag{3.43b}$$

where

$$F(x) = (R/l_m)^2\cos(x/R). \tag{3.44}$$

Here $l_m = \sqrt{\frac{\hbar}{eB_0}}$ is the magnetic length and the normalization constant N is given by

$$\begin{aligned} N^{-2} &= \int_0^L dx\, e^{2(R/l_m)^2\cos(x/R)} \\ &= RI_0(2R^2/l_m^2)/2\pi. \end{aligned} \tag{3.45}$$

I_0 is the modified Bessel function of the first kind, of order zero, and $\psi_\pm$ is normalized to identity, i.e.

$$\int_0^L dx\, \psi_\pm^\dagger(x)\psi_\pm(x) = 1. \tag{3.46}$$

3.3.2   Near-zero energy eigenstates with a small scalar potential

In the presence of a weak scalar potential U, the energy eigenstates near $\boldsymbol{k} = 0$ are studied by treating $H_1(\boldsymbol{k})$ as a perturbation. Perturbation theory is valid as long as the energy scales associated with the perturbation i.e. $\hbar v_F|\boldsymbol{k}|$ and U_0 are small compared to the level spacing of H_0. In the limit of weak magnetic field, i.e. $l_m \gg L$, the level spacing of H_0 is given by $\hbar v_F/R$. In the opposite limit, when $l_m \ll L$, the level spacing of H_0 is of the order $\hbar v_F/l_m$. We therefore expect perturbation theory to be accurate when $\hbar v_F|\boldsymbol{k}|$, $U_0 \ll \max\{\hbar v_F/l_m, \hbar v_F/R\}$.

Without the perturbation there are two eigenstates that are degenerate at zero energy. We therefore use degenerate first order perturbation theory. The eigenstates that solve $H(\boldsymbol{k})$ to first order in $\boldsymbol{k}$ and U_0 are

$$\Psi_{\boldsymbol{k}\pm} = \frac{e^{iky}}{\sqrt{\Lambda}}\left(\chi_{\boldsymbol{k}\pm}^+\psi_{0,+} + \chi_{\boldsymbol{k}\pm}^-\psi_{0,-}\right), \tag{3.47}$$

where the spinors $\chi_{\boldsymbol{k}\pm} = (\chi_{\boldsymbol{k}\pm}^+, \chi_{\boldsymbol{k}\pm}^-)^T$ satisfy

$$h(\boldsymbol{k})\chi_{\boldsymbol{k}\pm} = \epsilon_{\boldsymbol{k}\pm}\chi_{\boldsymbol{k}\pm}, \tag{3.48}$$

and $h(\boldsymbol{k})$ is a 2×2 matrix with the following matrix elements

$$h(\boldsymbol{k}) = \begin{pmatrix} h(\boldsymbol{k})_{++} & h(\boldsymbol{k})_{+-} \\ h(\boldsymbol{k})_{-+} & h(\boldsymbol{k})_{--} \end{pmatrix}. \tag{3.49}$$

Here $h(\boldsymbol{k})_{\sigma\sigma'} = \langle\psi_{0\sigma}|H_1(\boldsymbol{k})|\psi_{0\sigma'}\rangle$. Calculating $h(\boldsymbol{k})_{++}$ we find,

$$
\begin{aligned}
h(\boldsymbol{k})_{++} &= \int_0^L dx\, \psi_{0,+}^\dagger \left[\hbar v_F \boldsymbol{\sigma}\cdot(k\hat{\mathbf{x}} + k\hat{\mathbf{y}}) + U_0\cos\left(x/R\right)\right]\psi_{0,+} \\
&= \int_0^L dx\, N^2 \left(\begin{array}{cc} e^{(R/l_m)^2\cos(x/R)} & 0 \end{array} \right) \left(\begin{array}{cc} U_0\cos\left(x/R\right) & \hbar v_F(k_x - \imath k_y) \\ \hbar v_F(k_x + \imath k_y) & U_0\cos\left(x/R\right) \end{array} \right) \\
&\qquad\qquad\qquad \times \left(\begin{array}{c} e^{(R/l_m)^2\cos(x/R)} \\ 0 \end{array} \right) \\
&= \int_0^L dx\, N^2 \left(U_0\cos\left(x/R\right)e^{(R/l_m)^2\cos(x/R)} \right) \\
&= U_0\frac{I_1(2\alpha)}{I_0(2\alpha)}.
\end{aligned}
\tag{3.50}
$$

Here I_1 is the first order modified Bessel function of the first kind. The matrix element $h(\boldsymbol{k})_{--}$ is obtained with similar calculations and is found to be

$$
h(\boldsymbol{k})_{--} = -U_0\frac{I_1(2\alpha)}{I_0(2\alpha)}.
\tag{3.51}
$$

The matrix element $h(\boldsymbol{k})_{+-}$ is calculated as follows:

$$
\begin{aligned}
h(\boldsymbol{k})_{+-} &= \int_0^L dx\, \psi_{0,+}^\dagger \left[\hbar v_F \boldsymbol{\sigma}\cdot(k\hat{\mathbf{x}} + k\hat{\mathbf{y}}) + U_0\cos\left(x/R\right)\right]\psi_{0,-} \\
&= \int_0^L dx\, N^2 \left(\begin{array}{cc} e^{(R/l_m)^2\cos(x/R)} & 0 \end{array} \right) \left(\begin{array}{cc} U_0\cos\left(x/R\right) & \hbar v_F(k_x - \imath k_y) \\ \hbar v_F(k_x + \imath k_y) & U_0\cos\left(x/R\right) \end{array} \right) \\
&\qquad\qquad\qquad \times \left(\begin{array}{c} 0 \\ e^{-(R/l_m)^2\cos(x/R)} \end{array} \right) \\
&= \int_0^L dx\, N^2 \hbar v_F(k_x + \imath k_y) \\
&= \frac{\hbar v_F(k_x + \imath k_y)}{I_0(2R/l_m)}.
\end{aligned}
\tag{3.52}
$$

And $h(\boldsymbol{k})_{-+}$ is equal to the complex conjugate of $h(\boldsymbol{k})_{+-}$, so that

$$
h(\boldsymbol{k})_{-+} = \frac{\hbar v_F(k_x - \imath k_y)}{I_0(2R/l_m)}.
\tag{3.53}
$$

Substituting these matrix elements back into $h(\boldsymbol{k})$, we find

$$
h(\boldsymbol{k}) = (\hbar\tilde{v}_F\boldsymbol{\sigma}\cdot\boldsymbol{k} + \mu\sigma_z).
\tag{3.54}
$$

Here $\tilde{v}_F$ is the renormalized Fermi velocity

$$\tilde{v}_F = \frac{v_F}{I_0(2R^2/l_m^2)}, \tag{3.55}$$

and μ the effective mass

$$\mu = U_0 \frac{I_1(2R^2/l_m^2)}{I_0(2R^2/l_m^2)}. \tag{3.56}$$

The energy of the state is

$$\epsilon_{\boldsymbol{k}\pm} = \pm \epsilon_{\boldsymbol{k}} = \pm \sqrt{\mu^2 + (\hbar\tilde{v}_F \boldsymbol{k})^2}. \tag{3.57}$$

The corresponding eigenstates in the vicinity of $\boldsymbol{k} = 0$ are

$$\chi_{\boldsymbol{k}\pm} = \frac{1}{\sqrt{2}} \begin{pmatrix} \sqrt{1 \pm \frac{\mu}{\epsilon}} \\ \pm\sqrt{1 \mp \frac{\mu}{\epsilon}} e^{\imath\theta} \end{pmatrix}, \tag{3.58}$$

with $e^{\imath\theta} = \frac{1}{\sqrt{k_x^2+k_y^2}}(k_x + \imath k_y)$.

3.3.3   Analytical formalism for Hall conductance

We now use the approximate expressions for the eigenstates and energies obtained in the previous section and substitute them in the Kubo formula in order to calculate the Hall conductance. We start with the term containing σ_y,

$$\begin{aligned}
\left\langle \Psi_{\boldsymbol{k}_1^-} \middle| \sigma_y \middle| \Psi_{\boldsymbol{k}_2^+} \right\rangle &= \frac{1}{\Lambda} \int_0^\Lambda dy \int_0^L dx\, \Psi_{\boldsymbol{k}_1^-}(\boldsymbol{r})^\dagger \sigma_y \Psi_{\boldsymbol{k}_2^+}(\boldsymbol{r}) \\
&= \frac{1}{\Lambda} \int_0^\Lambda dy\, e^{-\imath(k_1-k_2)y} \int_0^L dx\, \psi_{\boldsymbol{k}_1^-}(x)^\dagger \sigma_y \psi_{\boldsymbol{k}_2^+}(x).
\end{aligned} \tag{3.59}$$

But $\frac{1}{\Lambda}\int_0^\Lambda dy\, e^{-\imath(k_1-k_2)y} = \delta_{k_1 k_2}$, so that

$$
\begin{aligned}
\left\langle \Psi_{\boldsymbol{k}_1^-}\middle|\sigma_y\middle|\Psi_{\boldsymbol{k}_2^+}\right\rangle &= \delta_{k_1 k_2}\int_0^L dx\,\psi_{\boldsymbol{k}_1^-}(x)^\dagger \sigma_y \psi_{\boldsymbol{k}_1^+}(x)\\
&= \delta_{k_1 k_2}\int_0^L dx\,(\chi_{\boldsymbol{k}-}^{+*}\psi_{0,+}^\dagger + \chi_{\boldsymbol{k}-}^{-*}\psi_{0,-}^\dagger)\sigma_y(\chi_{\boldsymbol{k}+}^+\psi_{0,+} + \chi_{\boldsymbol{k}+}^-\psi_{0,-})\\
&= \delta_{k_1 k_2}\int_0^L dx\, N^2 \left(\begin{array}{cc}\chi_{\boldsymbol{k}-}^{+*}e^{F(x)} & \chi_{\boldsymbol{k}-}^{-*}e^{-F(x)}\end{array}\right)\left(\begin{array}{c}-\imath\chi_{\boldsymbol{k}+}^+ e^{-F}(x)\\ \imath\chi_{\boldsymbol{k}+}^+ e^{F}(x)\end{array}\right) \quad (3.60)\\
&= LN^2\left(-\imath\chi_{\boldsymbol{k}-}^{+*}\chi_{\boldsymbol{k}+}^- + \imath\chi_{\boldsymbol{k}-}^{-*}\chi_{\boldsymbol{k}+}^+\right)\\
&= LN^2\chi_{\boldsymbol{k}-}^\dagger \sigma_y \chi_{\boldsymbol{k}+}.
\end{aligned}
$$

With similar calculations, the term in the Kubo containing σ_x is found to be

$$
\left\langle \psi_{\boldsymbol{k}_2^+}\middle|\sigma_x\middle|\psi_{\boldsymbol{k}_1^-}\right\rangle = \delta_{k_1 k_2}LN^2\chi_{\boldsymbol{k_1}+}^\dagger\sigma_x\chi_{\boldsymbol{k_2}-}. \tag{3.61}
$$

The δ function also implies that $\epsilon_1 = -\epsilon_2$, such that the term $(\epsilon_1-\epsilon_2)^2$ in the denominator of the Kubo formula, Equation (3.39), becomes $4\epsilon^2$. Substituting this and Equation (3.60) and Equation (3.61) back into the Kubo formula, we obtain

$$
\sigma_{yx}^\tau = \frac{2e^2}{h}\frac{(\hbar\tilde{v}_F)^2}{\Lambda R}\sum_{\boldsymbol{k}}\frac{\text{Im}\left\{\left[\chi_{\boldsymbol{k}-}^\dagger\sigma_y\chi_{\boldsymbol{k}+}\right]\left[\chi_{\boldsymbol{k}+}^\dagger\sigma_x\Psi_{\boldsymbol{k}-}\right]\right\}}{4\epsilon_{\boldsymbol{k}}^2}. \tag{3.62}
$$

Substituting the explicit form of the states $\chi_{\boldsymbol{k}\pm}$ in the equation above, the Kubo formula now becomes

$$
\sigma_{yx}^\tau = \frac{1}{2}\frac{e^2}{h}\frac{(\hbar\tilde{v}_F)^2}{\Lambda R}\sum_{\boldsymbol{k}}\frac{\mu}{\epsilon_k^3}. \tag{3.63}
$$

By substituting the value of the energy ϵ and replacing $\frac{1}{\Lambda}\sum_{k_y}$ with $\frac{1}{2\pi}\int_{-\infty}^\infty dk_y$, we obtain

$$
\begin{aligned}
\sigma_{yx}^\tau &= \frac{1}{2}\frac{e^2}{h}\frac{(\hbar\tilde{v}_F)^2}{2\pi R}\sum_{k_x}\int_{-\infty}^\infty dk_y\,\frac{\mu}{[\mu^2+(\hbar\tilde{v}_F k_x)^2+(\hbar\tilde{v}_F k_y)^2]^{\frac{3}{2}}}\\
&= \frac{1}{2}\frac{e^2}{h}\frac{(\hbar\tilde{v}_F)^2}{2\pi R}\sum_{k_x}\frac{\mu}{[\mu^2+(\hbar\tilde{v}_F k_x)^2]^{\frac{3}{2}}}\int_{-\infty}^\infty dk_y\left[1+\frac{(\hbar\tilde{v}_F k_y)^2}{\mu^2+(\hbar\tilde{v}_F k_x)^2}\right]^{-\frac{3}{2}}.
\end{aligned} \tag{3.64}
$$

To integrate Equation (3.64), let

$$
z = \frac{\hbar\tilde{v}_F k_y}{\sqrt{\mu^2+(\hbar\tilde{v}_F k_x)^2}}, \tag{3.65}
$$

and therefore

$$dz = \frac{\hbar \tilde{v}_F}{\sqrt{\mu^2 + (\hbar \tilde{v}_F k_x)^2}} dk_y. \tag{3.66}$$

Substituting Equation (3.65) and Equation (3.66) back into Equation (3.64) we obtain

$$\sigma_{yx}^{\tau} \;\; = \;\; \frac{1}{2} \frac{e^2}{h} \frac{(\hbar \tilde{v}_F)^2}{2\pi R} \sum_{k_x} \frac{\mu}{[\mu^2 + (\hbar \tilde{v}_F k_x)^2]^{\frac{3}{2}}} \int_{-\infty}^{\infty} dz \left(1 + z^2\right)^{-\frac{3}{2}}. \tag{3.67}$$

Here

$$\int_{-\infty}^{\infty} dz \left(1 + z^2\right)^{-\frac{3}{2}} = 2, \tag{3.68}$$

such that

$$\sigma_{yx}^{\tau} \;\; = \;\; \frac{e^2}{h} \frac{\hbar \tilde{v}_F}{2\pi R} \sum_{k_x} \frac{\mu}{\mu^2 + (\hbar \tilde{v}_F k_x)^2}. \tag{3.69}$$

Substituting the value for k_x from Equation (3.40) leads to

$$\sigma_{yx}^{\tau} = \frac{e^2}{h} \frac{\hbar \tilde{v}_F}{2\pi R} \sum_{m} \frac{\mu}{\mu^2 + (\hbar \tilde{v}_F)^2 \left(\frac{m}{R} + \frac{\theta - 2\pi v\tau/3}{2\pi R}\right)^2}. \tag{3.70}$$

Setting $\gamma = 2\pi R \mu / \hbar \tilde{v}_F$ and summing the contribution from the two valleys, the analytical formula for the Hall conductance is

$$\sigma_{yx} = \frac{e^2}{h} \sum_{m} \left[\frac{\gamma}{\gamma^2 + (2\pi m + \theta - 2\pi \nu/3)^2} + \frac{\gamma}{\gamma^2 + (2\pi m + \theta + 2\pi \nu/3)^2} \right]. \tag{3.71}$$

Further simplification of Equation (3.71) is possible in the small and large γ limits. We shall now consider these two situations.

3.3.4 Results

In the limit of $\gamma \ll 2\pi$, all but the term with the smallest denominator in Equation (3.71) make a negligible contribution to the sum. Realizing that $\nu = 0$ for metallic carbon nanotubes, the Hall conductance expressed as a function of θ consists out of a sequence of Lorentzian peaks at $\theta = 2\pi m$, where m takes on values equal to $0, \pm 1, \pm 2, \ldots$. The height of each of the peaks, when we consider a metallic tube, is equal to $2e^2/\gamma h$ and the width equal to γ. For semi-conducting

tubes, $\nu = \pm 1$ and there are two sequences of Lorentzian peaks at $\theta = 2\pi m \pm 2\pi/3$. The peak heights are equal to $e^2/\gamma h$ and the peak widths are given by γ.

When $\gamma \gg 2\pi$ the sum in Equation (3.71) can be converted into an integral and the Hall conductance now becomes

$$\sigma_{yx}^{\gamma \gg 2\pi} = \frac{e^2}{h}, \tag{3.72}$$

i.e. the Hall conductance becomes quantized and independent of the flux θ. This can be understood as follows: eigenstates in the vicinity of the Dirac point are localized on the scale of l_m and therefore become insensitive to the boundary condition when $l_m < R$. Because θ only appears in the boundary condition, the analytical formula for the Hall conductance becomes independent of θ when $\gamma \gg 2\pi$.

There is however another form of quantization that remains valid regardless of the magnitude of R/l_m, namely the average of $\sigma_{yx}(\theta)$, i.e.

$$\langle \sigma_{yx} \rangle_\theta = \int_0^{2\pi} d\theta \, \sigma_{yx}(\theta)/2\pi, \tag{3.73}$$

is always quantized. The expected quantization of the average is therefore obeyed:

$$\langle \sigma_{yx} \rangle_\theta = e^2/h. \tag{3.74}$$

This result is derived in the small U_0 limit, but we have shown in Chapter 2 that $\langle \sigma_{yx} \rangle_\theta$ equals an integer multiple of e^2/h even beyond this regime [15]. We have shown that there is a region around $U_0 = 0$ where this integer equals one, as opposed to the trivial case where it is zero.

3.3.5 Amount of electrons transported between the ends of the tube

When the flux through the tube is varied by one flux quantum, exactly one electron is transported between the ends of the tube. This can be explained as follows. Faraday's law states that the rate of change of the magnetic flux is equal to the emf generated. Thus if the flux, Φ, threading the carbon nanotube tube is varied, an emf around the circumference of the tube is

produced:

$$-\frac{d\Phi}{dt} = \frac{h}{e}\frac{d\theta}{dt}. \tag{3.75}$$

Because the Hall conductance is non-zero, a current I is produced along the the axis of the tube, such that

$$\begin{aligned} I_y &= \sigma_{yx}(\theta)\left(-\frac{d\Phi}{dt}\right) \\ &= \sigma_{yx}(\theta)\left(\frac{h}{e}\frac{d\theta}{dt}\right). \end{aligned} \tag{3.76}$$

If we vary the flux by one flux quantum between $t = 0$ and $t = t_0$, the total charge that is transported through the cross-section of the tube from time zero to time t_0 is

$$Q = \int_0^{t_0} dt\, I. \tag{3.77}$$

Substituting Equation (3.76) into Equation (3.77):

$$\begin{aligned} Q &= \int_0^{t_0} dt\,\sigma_{yx}(\theta)\left(\frac{h}{e}\frac{d\theta}{dt}\right) \\ &= \frac{h}{e}\int_0^{2\pi} d\theta\,\sigma_{yx}(\theta). \end{aligned} \tag{3.78}$$

From Equation (3.74) follows:

$$\begin{aligned} Q &= \frac{h}{e} \times \frac{e^2}{h} \\ &= e. \end{aligned} \tag{3.79}$$

Therefore, when the flux is varied with one flux quantum, exactly one electron per spin is transported through the tube.

We conclude this chapter by briefly considering the assumptions we made in order to achieve our results. This also serves as motivation for the numerical work that will be presented in the next chapter. To obtain our analytical results, we made two assumptions: firstly we assumed that first order perturbation theory in $\boldsymbol{k}$ and U_0 is accurate for all modes that contribute to σ_{yx}. Secondly we assumed that the modes in the sum of Equation (3.71) for which first order perturbation theory is not accurate, give negligible contribution. In the next chapter we shall compare these results with numerical calculations to see if these assumptions place a restriction

on the strength of the magnetic field for which Equation (3.71) is valid.

CHAPTER 4
Numerical calculation

4.1   Numerical representation

In Chapter 3 we analytically calculated the Hall conductance of a carbon nanotube under the influence of a magnetic field and electric field parallel to each other, but perpendicular to the tube axis. We applied an additional magnetic field parallel to the tube axis, so that the flux, Φ, may be varied. The analytical results were obtained with perturbation theory. For perturbation theory to be valid we inevitably had to make curtain assumptions. These assumptions may have an influence on the range of applicability of the results. With the range of applicability we imply that there may by certain values of the system parameters, namely the strength of the magnetic field, the strength of the scalar potential and the magnetic flux, where the perturbative results are inaccurate. The goal of this chapter is therefore to test the accuracy of the perturbative results and investigate under what conditions these results are valid.

The strategy of this chapter is firstly to represent the nearest neighbor tight binding Hamiltonian for a carbon nanotube, in a matrix form. We then show that through translation invariance along the length of the tube, it is not necessary to numerically diagonalize the entire Hamiltonian at once. Numerical results for the eigenstates and energies are found by diagonalizing a much smaller matrix in comparison to the total Hamiltonian. The eigenvalues and eigenstates are substituted into the Kubo formula to obtain numerical results for the Hall conductance. Lastly we compare the exact, numerical results for the Hall conductance with the approximate analytical results obtained in Chapter 3. We also investigate the behavior of the gap between the valence band and the conduction band as a function of the system parameters and obtain the conditions under which the perturbative results are accurate or inaccurate.

As we already discussed, a graphene sheet consists of a lattice of carbon atoms positioned on the vertices of a hexagon. Electrons can hop from a carbon atom to its nearest neighbor on the path that connects these carbon atoms. To describe the hopping of the electrons from one lattice point to the other, we use a more convenient lattice than the hexagonal lattice. The square lattice is much simpler to implement in the numerical calculation and can be deformed to describe the hexagonal lattice. By setting certain hopping elements, that connects the different columns with each other in the square lattice to zero, the so called "brick-wall lattice" is obtained. The brick-
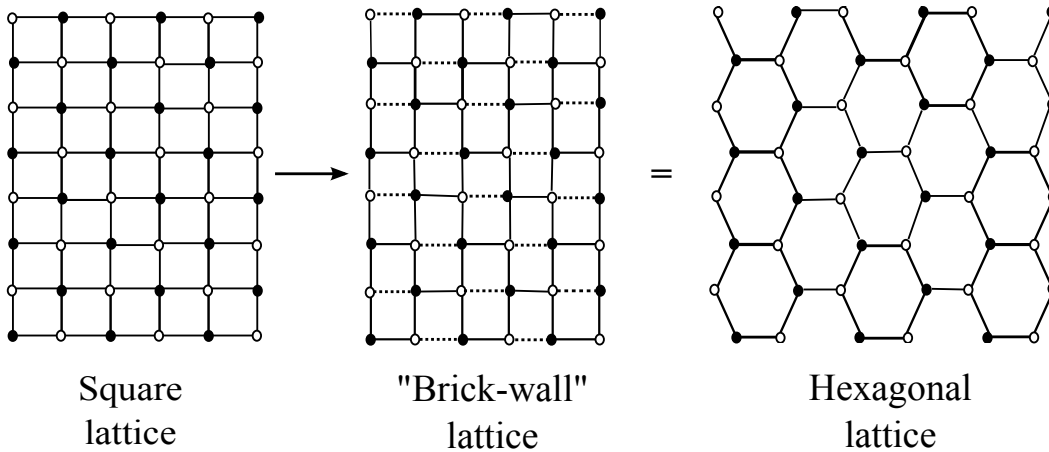
Figure 4.1: Illustration of how the brick-wall lattice is used to describe the hexagonal lattice of graphene. Setting certain hopping elements in the square lattice to zero allows one to obtain the brick-wall lattice, which has the same topology as the honeycomb lattice.

wall lattice is topologically equivalent to the hexagonal lattice, but it retains the more convenient shape of the square lattice. In Figure 4.1 we show how the square lattice is transformed into the brick-wall lattice and how the brick-wall lattice corresponds to the hexagonal lattice of graphene.

4.1.1   Labeling the graphene lattice

Consider a brick wall lattice with M rows and $2N$ columns. The way we label the graphene sheet, is explained in Figure 4.2. We indicate the two basis atoms, A and B with a white and black dot, respectively. By examining the columns of the lattice, one notices only two types of columns with the same sequence of A and B-labeled carbon atoms exists. Therefore the entire graphene lattice consists of out replicas of only two different types of columns, which we label as $\eta = 1$ and $\eta = 2$. The n'th pair of columns (that consist out of $\eta = 1$ and $\eta = 2$) is grouped together and we label them as n. There exists $n = 1, ..., N$ such pairs. Therefore each atom is labeled by a row index $m = 1, .., M$, a column index $n \in 1, .., N$ and a pair index $\eta \in 1, 2$.

4.1.2   Carbon nanotube constructed out of a graphene sheet

Thus far we explained the hexagonal lattice in terms of a more convenient lattice and introduced the labeling scheme for a graphene sheet. However, the system that we investigate is a carbon nanotube. A carbon nanotube has the same assembly of carbon atoms arranged in a hexagonal lattice as for the graphene sheet, but has a cylindric structure. We now use the
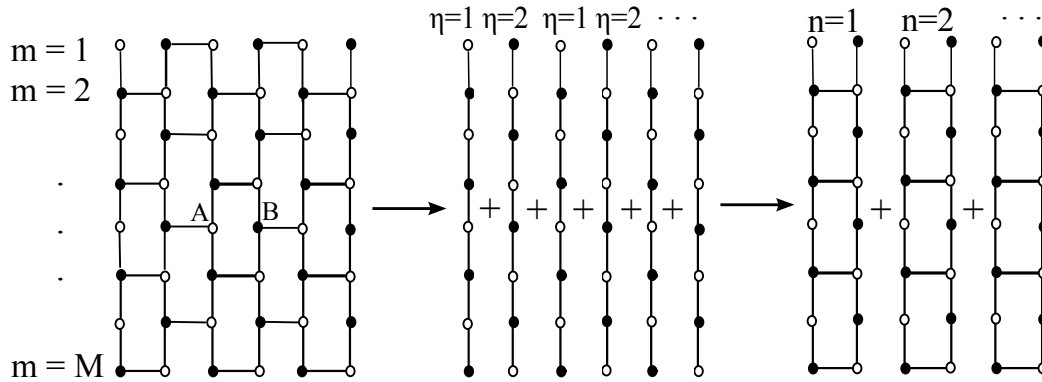
Figure 4.2: Dividing the graphene sheet into single columns, one notices that the graphene lattice consists out of a sequence of replicas of only two different types of columns, $\eta = 1$ and $\eta = 2$.

labeling scheme to explain how this cylindrical structure of the carbon nanotube is obtained.

Imagine taking a graphene sheet and rolling it up to form a cylinder and reconnect the first carbon atom ($m = 1$) and the last carbon atom ($m = M$) of every column in the graphene sheet. Subsequently every column in the lattice now forms a ring and very ring has the same amount of sites $m = 1, 2, ..., M$ along the circumference.

4.2   Hamiltonian matrix

To numerically calculate the eigenvalues and eigenstates of the carbon nanotube, the tight binding Hamiltonian needs to be presented in a matrix form. In this section we show how the on-site energies and the hopping parameters containing the magnetic field of a carbon nanotube (within the nearest neighbor approach) is expressed in matrix form.

4.2.1   Matrix representation of the tight binding Hamiltonian

We begin this discussion by defining the state vectors of the system in position representation. A single particle wave function represents the probability amplitude for finding a particle at an individual point of the lattice. For a system with M rows and $2N$ columns, the state vector is a vector with $2N \times M$ entries. We rearrange the entries as follows. The state vector Ψ is divided

into N sub-vectors, each with $2M$ entries:

$$\Psi = \begin{pmatrix} \Psi_1 \\ \Psi_2 \\ \vdots \\ \Psi_N \end{pmatrix}. \tag{4.1}$$

The vector Ψ_n contains the amplitudes of finding the particle at the nth "two-ring-pair" as defined in Figure (3.2). We arrange the entries of Ψ_n so that the amplitude of the lattice point, $(\eta - 1)M + m$ is equal to the entry ηm of Ψ_n. As before, we consider tubes that are long enough that the boundary condition in the longitudinal direction does not affect the result. We therefore choose the most convenient boundary conditions, namely periodic boundary conditions. In this representation of the states, the Hamiltonian is a $2MN \times 2MN$ matrix. The matrix is block tri-diagonal and the size of each block is $M \times M$.

$$H = \begin{pmatrix} H_1 & t_0^* & 0 & \cdots & & 0 & t_{0'} \\ t_0 & H_2 & t_{0'}^* & 0 & \cdots & & 0 \\ 0 & t_{0'} & H_1 & t_0^* & 0 & \cdots & 0 \\ \vdots & & & \ddots & & & \vdots \\ 0 & & \cdots & & 0 & H_1 & t_0^* \\ t_{0'}^* & 0 & \cdots & & 0 & t_0 & H_2 \end{pmatrix}_{2N \times 2N} . \tag{4.2}$$

The off-diagonal blocks in the Hamiltonian H describe the hopping between different rings. There are two types of coupling matrices between the sub-matrices, namely t_0 and $t_{0'}$. These two coupling matrices are diagonal, the entries on the diagonal are given by:

$$t_{0'} = \begin{pmatrix} t_0(1) & & & & & \\ & 0 & & & & 0 \\ & & t_0(3) & & & \\ & & & 0 & & \\ & & & & \ddots & \\ & 0 & & & & t_0(M-1) \\ & & & & & & 0 \end{pmatrix}_{M \times M} , \tag{4.3}$$

and

$$
t_0 \;=\; \begin{pmatrix}
0 & & & & & \\
& t_0(2) & & & 0 & \\
& & 0 & & & \\
& & & t_0(4) & & \\
& & & & \ddots & \\
& 0 & & & & 0 \\
& & & & & & t_0(M)
\end{pmatrix}_{M \times M} .
\tag{4.4}
$$

The diagonal entries of t_0 and $t_{0'}$, in terms of the the carbon atom number m, where $m = 1, 2, ..., M$, is derived as follows: We start with the definition of the hopping amplitude, t_0, Equation (2.7):

$$
t_0 = t e^{i\gamma_0},
\tag{4.5}
$$

where the phase γ_0, Equation (2.9a), is chosen to be

$$
\gamma_0 = -\frac{\sqrt{3}}{4} \frac{ea}{\hbar} A_y(\boldsymbol{r}).
\tag{4.6}
$$

If we substitute this back into the definition of t_0 we obtain:

$$
t_0 = t e^{-i\frac{\sqrt{3}}{4}\frac{ea}{\hbar}A_y(\boldsymbol{r})}.
\tag{4.7}
$$

The total vector potential is given by:

$$
\boldsymbol{A} = B_0 \frac{L}{2\pi} \sin\left(\frac{2\pi x}{L}\right) \hat{y} + \frac{\Phi}{2\pi L} \hat{x},
\tag{4.8}
$$

and includes both the magnetic field perpendicular to the tube axis (first term) and the magnetic field parallel to the tube axis (second term). For t_0 we are only interested in $\boldsymbol{y}$ component of the total vector potential. If we now substitute Equation (4.8) into Equation (4.7) we obtain:

$$
t_0 = e^{-i\frac{\sqrt{3}}{8\pi}\frac{eaL}{\hbar}B_0 \sin\left(\frac{2\pi x}{L}\right)},
\tag{4.9}
$$

Let each carbon atom m be positioned at the corresponding x position, such that carbon atom number $m = 1$ is positioned at $x = a$ and carbon number $m = Ma$ positioned at $x = M$. We

can therefore write:

$$t_0(m) = e^{-i\frac{\sqrt{3}}{8\pi}\frac{eaL}{\hbar}B_0\sin\left(\frac{2\pi ma}{L}\right)}.$$ (4.10)

The two matrices t_0 and $t_{0'}$ represents the hopping in the longitudinal direction of the tube from a B-labeled carbon atom in one ring to an A-labeled carbon atom in the other ring of the pair. The only difference between t_0 and $t_{0'}$ is that $t_{0'}$ describes the hopping between a ring of type $\eta = 1$ on the left to a ring of type $\eta = 2$ on the right, whereas t_0 describes how electrons hop from a ring of type $\eta = 2$ on the left to a ring of type $\eta = 1$ on the right. This is illustrated in Figure 4.3.

Figure 4.3: **The hopping amplitude t_0' describes the hopping between a ring of type $\eta = 1$ on the left to a ring $\eta = 2$ on the right, and the hopping amplitude t_0 describes how electrons hop from a ring of type $\eta = 2$ on the left to a ring of type $\eta = 1$ on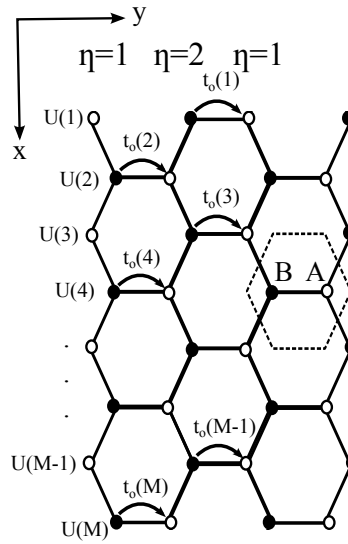 the right. The hopping amplitudes are defined in terms of vectors connecting a B-carbon atom to its nearest neighbors, which are all A-carbon atoms.**

The diagonal blocks in H describes the hopping of the carbon atoms within each ring, i.e.

along the circumference of the carbon nanotube and is given by:

$$H_1 = \begin{pmatrix} U(1) & t_2(1) & 0 & \cdots & & 0 & t_1(1) \\ t_2^*(1) & U(2) & t_1^*(3) & 0 & \cdots & & 0 \\ 0 & t_1(3) & U(3) & t_2(3) & 0 & \cdots & 0 \\ \vdots & & & \ddots & & & \vdots \\ 0 & \cdots & 0 & t_1(M-1) & U(M-1) & t_2(M-1) \\ t_1^*(1) & 0 & \cdots & & 0 & t_2^*(M-1) & U(M) \end{pmatrix}_{M \times M} \tag{4.11a}$$

and

$$H_2 = \begin{pmatrix} U(1) & t_1^*(2) & 0 & \cdots & & 0 & t_2^*(M) \\ t_1(2) & U(2) & t_2(2) & 0 & \cdots & & 0 \\ 0 & t_2^*(2) & U(3) & t_1^*(4) & 0 & \cdots & 0 \\ \vdots & & & \ddots & & & \vdots \\ 0 & \cdots & 0 & t_2^*(M-2) & U(M-1) & t_1^*(M) \\ t_2(M) & 0 & \cdots & & 0 & t_1(M) & U(M) \end{pmatrix}_{M \times M}. \tag{4.11b}$$

The on-site potential energy $U(m)$, on the diagonal of H_1 and H_2, varies only in the transverse direction (x-direction) and is constant in the longitudinal direction (y-direction) of the carbon nanotube. This is illustrated in Figure 4.4. The explicit expression for $U(m)$ is given by

$$U(m) = U_0 \sin\left(\frac{2\pi}{M}m\right). \tag{4.12}$$

The hopping amplitudes $t_1(m)$ and $t_2(m)$ couples a carbon atom to its nearest neighbors around the circumference. The expressions for these two hopping amplitudes are derived as follows: The definition of the hopping amplitudes, t_1 and t_2 are given by Equation (2.7):
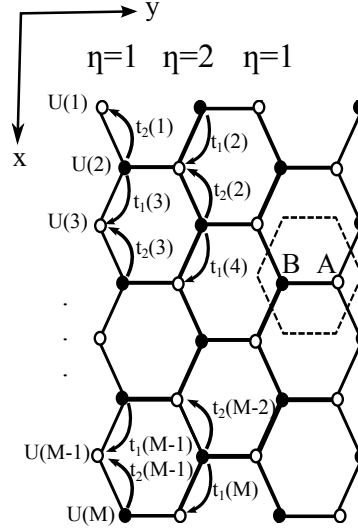
$$t_j = te^{i\gamma_j}, \tag{4.13}$$

Figure 4.4: The hopping amplitude t_1 describes the hopping from a B labeled atom to a A labeled atom in the x-direction and the hopping amplitude t_2 describes the hopping from a B labeled atom to a A labeled atom in the $-x$-direction.

where $j = 1, 2$. In Chapter 2 we showed that the phases γ_1 and γ_2 are chosen to be:

$$\gamma_1 = \frac{\sqrt{3}}{4}\frac{ea}{\hbar}A_y(\boldsymbol{r}) + \frac{ea}{2\hbar}A_x(\boldsymbol{r}), \tag{4.14a}$$

$$\gamma_2 = \frac{\sqrt{3}}{4}\frac{ea}{\hbar}A_y(\boldsymbol{r}) - \frac{ea}{2\hbar}A_x(\boldsymbol{r}), \tag{4.14b}$$

If we substitute this back into Equation (4.13) we obtain:

$$t_1 = te^{\imath\frac{\sqrt{3}}{4}\frac{ea}{\hbar}A_y(\boldsymbol{r})}e^{\imath\frac{ea}{2\hbar}A_x(\boldsymbol{r})}, \tag{4.15}$$

$$t_2 = te^{\imath\frac{\sqrt{3}}{4}\frac{ea}{\hbar}A_y(\boldsymbol{r})}e^{-\imath\frac{ea}{2\hbar}A_x(\boldsymbol{r})}. \tag{4.16}$$

By substituting the total vector potential, Equation (4.8) into the equations above, we obtain the expressions for t_1 and t_2 as a function of $m = 1, ..., M$, (the carbon atom number),

$$t_1 = e^{\imath\frac{\sqrt{3}}{8\pi}\frac{eL}{\hbar}B_0\cos\left(\frac{2\pi m}{M}\right)}e^{\imath\theta/2(M+1)}, \tag{4.17a}$$

and

$$t_2 = e^{\imath\frac{\sqrt{3}}{8\pi}\frac{eL}{\hbar}B_0\cos\left(\frac{2\pi m}{M}m\right)}e^{-\imath\theta/2(M+1)}. \tag{4.17b}$$

4.2.2 Translation invariance

Due to translation invariance along the length of the tube, it is not necessary to numerically diagonalize the $2NM \times 2NM$ matrix, Equation (4.2). We only need to diagonalize a $2M \times 2M$ matrix. This can be explained as follows. We identify the following two matrices D and T:

$$D = \begin{pmatrix} H_1 & T_0^{\dagger} \\ T_0 & H_2 \end{pmatrix}_{2M \times 2M}, \tag{4.18a}$$

$$T = \begin{pmatrix} 0 & t_{0'} \\ 0 & 0 \end{pmatrix}_{2M \times 2M}. \tag{4.18b}$$

The Hamiltonian H, in terms of these two matrices is

$$H = \begin{pmatrix} D & T^{\dagger} & 0 & \cdots & & 0 & T \\ T & D & T^{\dagger} & 0 & \cdots & & 0 \\ 0 & T & D & T^{\dagger} & 0 & \cdots & 0 \\ \vdots & & & \ddots & & & \vdots \\ 0 & \cdots & & 0 & T & D & T^{\dagger} \\ T & 0 & \cdots & & 0 & T & D \end{pmatrix}_{N \times N}. \tag{4.19}$$

Due to the periodic boundary conditions in the longitudinal direction of the tube, the state vector Ψ_0 is equal to the state vector Ψ_N, so that the eigenvalue equation $E\Psi = H\Psi$ becomes

$$E\Psi_n = T\Psi_{n-1} + D\Psi_n + T^{\dagger}\Psi_{n+1}. \tag{4.20}$$

We are now able to Fourier transform Equation (4.20) from position space to momentum space. We make the following ansatz for the wave function Ψ_n:

$$\Psi_n = e^{ikn}\phi_k, \tag{4.21}$$

where $n = 1, ..., N$ and ϕ_k is a $2M$ dimensional vector independent of n. The wave number k is given by

$$k = 2\pi n/N. \tag{4.22}$$

Substituting the ansatz in Equation (4.20), one finds that ϕ_k solves the eigenvalue equation $E_k \phi_k = H_k \phi_k$, where E_k is the eigenvalue of H. The effective Hamiltonian H_k, is given by

$$H_k = (T e^{-ik} + D + T^\dagger e^{ik}), \tag{4.23}$$

and has a dimension of $2M \times 2M$. This is much smaller than the total Hamiltonian H with a dimension $2MN \times 2MN$. We are thus able to consider larger systems because we only need to numerically diagonalize the effective Hamiltonian. The eigenvalues and energies obtained are then substituted into the Kubo formula to calculate the Hall conductance.

In the following section we show how to calculate the Hall conductance by using the eigenvalues and energies that we obtained in this section. The Hall conductance is calculated using the Kubo formula.

4.3 The Kubo formula

The Kubo formula gives us the Hall conductance in the form:

$$\sigma_{xy} = \frac{e^2 \hbar}{\imath A} \sum_{E_{kl} < 0 < E_{k'l'}} \frac{\left(\Psi_{kl}^\dagger v_x \Psi_{k'l'}\right)\left(\Psi_{k'l'}^\dagger v_y \Psi_{kl}\right) - \left(\Psi_{kl}^\dagger v_y \Psi_{k'l'}\right)\left(\Psi_{k'l'}^\dagger v_x \Psi_{kl}\right)}{(E_{kl} - E_{k'l'})^2}. \tag{4.24}$$

Here the eigenstates Ψ_{kl} and $\Psi_{k'l'}$ are the eigenstates corresponding to the energies E_{kl} and $E_{k'l'}$. The energy E_{kl} represents the energies smaller than the Fermi energy and $E_{k'l'}$ is the energies bigger than the Fermi energy. The Fermi energy is chosen to be equal to zero. A is the surface area of the tube wall and v_x and v_y are the velocity operators. The velocity operators are derived in Chapter 2 and is explicitly given by:

$$\vec{v} = -\frac{i}{\hbar} \sum_{n,m} \boldsymbol{d}_{n,m} t_{n,m} |n\rangle \langle m| . \tag{4.25}$$

In order to numerically calculate the Hall conductivity, we have to calculate the matrix elements of the velocity operators. We start by presenting the explicit expressions of the velocity operators.

4.3.1   The velocity operators

The velocity of the electrons in the x direction is described by the following block matrix

$$v_x = \begin{pmatrix} v_{x1} & & & & & \\ & v_{x2} & & 0 & & \\ & & \ddots & & & \\ & 0 & & v_{x1} & & \\ & & & & v_{x2} & \end{pmatrix}_{2N \times 2N} , \tag{4.26}$$

where v_{x1} and v_{x2} are $M \times M$ block matrices. The two sub matrices v_{x1} and v_{x2}, respectively describes the velocity of the electrons in the x-direction in a ring of type $\eta = 1$ and in a ring of type $\eta = 2$. Explicitly, v_{x1} and v_{x2} is given by:

$$v_{x1} = \frac{ia}{2\hbar} \begin{pmatrix} 0 & t_2(1) & 0 & \cdots & & & 0 & -t_1(1) \\ -t_2^*(1) & 0 & t_1^*(3) & 0 & \cdots & & & 0 \\ 0 & -t_1(3) & 0 & t_2(3) & 0 & & \cdots & 0 \\ \vdots & & & \ddots & & & & \vdots \\ 0 & \cdots & & 0 & -t_1(M-1) & 0 & t_2(M-1) \\ t_1^*(1) & 0 & \cdots & & 0 & -t_2^*(M-1) & 0 \end{pmatrix} \tag{4.27a}$$

and

$$v_{x2} = \frac{ia}{2\hbar} \begin{pmatrix} 0 & t_1^*(2) & 0 & \cdots & & & 0 & -t_2^*(M) \\ -t_1(2) & 0 & t_2(2) & 0 & \cdots & & & 0 \\ 0 & -t_2^*(2) & 0 & t_1^*(4) & 0 & & \cdots & 0 \\ \vdots & & & \ddots & & & & \vdots \\ 0 & \cdots & & 0 & -t_2^*(M-2) & 0 & t_1^*(M) \\ t_2(M) & 0 & \cdots & & 0 & -t_1(M) & 0 \end{pmatrix} . \tag{4.27b}$$

4. Numerical calculation

The hopping amplitudes t_1 and t_2 are the hopping amplitudes defined in Equation (4.17a) and Equation (4.17b).

The velocity of the electrons in the y-direction is described by:

$$
v_y = \begin{pmatrix}
v_{y1} & W_1 & 0 & \cdots & & 0 & W_2^\dagger \\
W_1^\dagger & v_{y2} & W_2 & 0 & \cdots & & 0 \\
0 & W_2^\dagger & v_{y1} & W_1 & 0 & \cdots & 0 \\
\vdots & & & \ddots & & & \vdots \\
0 & \cdots & & 0 & W_2^\dagger & v_{y1} & W_1 \\
W_2 & 0 & \cdots & & 0 & W_1^\dagger & v_{y2}
\end{pmatrix}_{2N \times 2N}
\tag{4.28}
$$

All of the following sub matrices have a dimension of $M \times M$ and are explicitly given by

$$
v_{y1} = \frac{ia}{2\sqrt{3}\hbar} \begin{pmatrix}
0 & t_2(1) & 0 & \cdots & & & 0 & t_1(1) \\
-t_2^*(1) & 0 & -t_1^*(3) & 0 & \cdots & & & 0 \\
0 & t_1(3) & 0 & t_2(3) & 0 & & \cdots & 0 \\
\vdots & & & & \ddots & & & \vdots \\
0 & \cdots & & 0 & t_1(M-1) & 0 & t_2(M-1) \\
-t_1^*(1) & 0 & \cdots & & & 0 & -t_2^*(M-1) & 0
\end{pmatrix},
\tag{4.29a}
$$

$$
v_{y2} = \frac{ia}{2\sqrt{3}\hbar} \begin{pmatrix}
0 & -t_1^*(2) & 0 & \cdots & & & 0 & -t_2^*(M) \\
t_1(2) & 0 & t_2(2) & 0 & \cdots & & & 0 \\
0 & -t_2^*(2) & 0 & -t_1^*(4) & 0 & & \cdots & 0 \\
\vdots & & & & \ddots & & & \vdots \\
0 & \cdots & & 0 & -t_2^*(M-2) & 0 & -t_1^*(M) \\
t_2(M) & 0 & \cdots & & & 0 & t_1(M) & 0
\end{pmatrix},
\tag{4.29b}
$$

$$
W_1 \;=\; \frac{ia}{\sqrt{3}\hbar}
\begin{pmatrix}
0 & & & & & \\
& t_0(2) & & & & 0 \\
& & 0 & & & \\
& & & t_0(4) & & \\
& & & & \ddots & \\
& 0 & & & & 0 \\
& & & & & t_0(M)
\end{pmatrix},
\tag{4.29c}
$$

and

$$
W_2 \;=\; \frac{ia}{\sqrt{3}\hbar}
\begin{pmatrix}
t_0(1) & & & & & \\
& 0 & & & & 0 \\
& & t_0(3) & & & \\
& & & 0 & & \\
& & & & \ddots & \\
& 0 & & & & t_0(M-1) \\
& & & & & & 0
\end{pmatrix}.
\tag{4.29d}
$$

4.3.2   Matrix elements of velocity operators

The next step is to calculate the matrix elements of the velocity operators so that they may be substituted into the Kubo formula. For this purpose it is convenient to divide the velocity operators v_x and v_y into $2M \times 2M$ sub-blocks. For the velocity operator in the y-direction, this is accomplished by defining the following two matrices

$$
A \;=\;
\begin{pmatrix}
v_{y1} & W_1 \\
W_1^{\dagger} & v_{y2}
\end{pmatrix}_{2M \times 2M},
\tag{4.30a}
$$

and

$$
B \;=\;
\begin{pmatrix}
0 & 0 \\
W_2 & 0
\end{pmatrix}_{2M \times 2M}.
\tag{4.30b}
$$

The velocity operator v_y in terms of these two matrices is

$$
v_y \;=\;
\begin{pmatrix}
A & B & 0 & \cdots & & 0 & B^\dagger \\
B^\dagger & A & B & 0 & \cdots & & 0 \\
0 & B^\dagger & A & B & 0 & \cdots & 0 \\
 & & & & & & \\
\vdots & & & \ddots & & & \vdots \\
 & & & & & & \\
0 & \cdots & & 0 & B^\dagger & A & B \\
B & 0 & \cdots & & 0 & B^\dagger & A
\end{pmatrix}_{N \times N}
. \tag{4.31}
$$

We now examine the term $\Psi^\dagger_{k'l'} v_y \Psi_{kl}$, which appears in the Kubo formula. Consider the nth, $2M$ dimensional sub-vector of $v_y \Psi_{kl}$:

$$
\begin{aligned}
(v_y \Psi_{kl})_n &= B^\dagger (\Psi_{kl})_{n-1} + A(\Psi_{kl})_n + B(\Psi_{kl})_{n+1} \\
&= \frac{e^{\imath k n}}{\sqrt{N}} \left(e^{-\imath k} B^\dagger + A + e^{\imath k} B \right) \phi_{kl}.
\end{aligned} \tag{4.32}
$$

Thus, the inner product $\Psi^\dagger_{k'l'} v_y \Psi_{kl}$ is given by:

$$
\begin{aligned}
\Psi^\dagger_{k'l'} v_y \Psi_{kl} &= \sum_{n=1}^{N} (\Psi_{k'l'})^\dagger_n (v_y \Psi_{kl})_n \\
&= \frac{1}{N} \left(\sum_{n=1}^{N} e^{\imath(k-k')n} \right) \phi^\dagger_{k'l'} \left(e^{-\imath k} B^\dagger + A + e^{\imath k} B \right) \phi_{kl} \\
&= \delta_{kk'} \phi^\dagger_{k'l'} \left(e^{-\imath k} B^\dagger + A + e^{\imath k} B \right) \phi_{kl} \\
&= \delta_{kk'} \phi^\dagger_{k'l'} \begin{pmatrix} v_{y1} & W_1 + e^{-ik} W_2^\dagger \\ W_1^\dagger + e^{ik} W_2 & v_{y2} \end{pmatrix} \phi_{kl}.
\end{aligned} \tag{4.33}
$$

We now define

$$
u_y(k) = \begin{pmatrix} v_{y1} & W_1 + e^{-ik} W_2^\dagger \\ W_1^\dagger + e^{ik} W_2 & v_{y2} \end{pmatrix}, \tag{4.34}
$$

such that

$$
\Psi^\dagger_{k'l'} v_y \Psi_{kl} = \delta_{kk'} \phi^\dagger_{k'l'} u_y(k) \phi_{kl}. \tag{4.35}
$$

The inner-product $\Psi_{kl}^{\dagger} v_y \Psi_{k'l'}$ is the Hermitian conjugate of $\Psi_{k'l'}^{\dagger} v_y \Psi_{kl}$ and is given by:

$$
\begin{aligned}
\Psi_{kl}^{\dagger} v_y \Psi_{k'l'} &= \left(\Psi_{k'l'}^{\dagger} v_y \Psi_{kl} \right)^{\dagger} \\
&= \delta_{kk'} \phi_{kl}^{\dagger} u_y(k) \phi_{kl'}.
\end{aligned}
\tag{4.36}
$$

To calculate the following two inner products $\Psi_{k'l'}^{\dagger} v_x \Psi_{kl}$ and $\Psi_{kl}^{\dagger} v_x \Psi_{k'l'}$, we now define the following matrix:

$$
C = \begin{pmatrix} v_{x1} & 0 \\ 0 & v_{x2} \end{pmatrix}_{2M \times 2M}.
\tag{4.37}
$$

The velocity operator in the x-direction in terms of the matrix above is diagonal, so that

$$
v_x = \begin{pmatrix} C & & & & \\ & C & & 0 & \\ & & \ddots & & \\ & 0 & & C & \\ & & & & C \end{pmatrix}_{N \times N}.
\tag{4.38}
$$

Similar calculations as for the term $\Psi_{k'l'}^{\dagger} v_y \Psi_{kl}$ above, yield

$$
\Psi_{k'l'}^{\dagger} v_x \Psi_{kl} = \delta_{kk'} \phi_{kl'}^{\dagger} u_x \phi_{kl},
\tag{4.39}
$$

and

$$
\Psi_{kl}^{\dagger} v_x \Psi_{k'l'} = \delta_{kk'} \phi_{kl}^{\dagger} u_x \phi_{kl'},
\tag{4.40}
$$

where

$$
u_x = \begin{pmatrix} v_{x1} & 0 \\ 0 & v_{x2} \end{pmatrix}.
\tag{4.41}
$$

We can now substitute Equation (4.35), Equation (4.36), Equation (4.39) and Equation (4.40) into the Kubo formula, Equation (4.24) to obtain the Hall conductivity in the form:

$$
\sigma_{xy} = \delta_{kk'} \frac{e^2 \hbar}{\imath A} \sum_k \sum_{l:E_{kl}<0} \sum_{l':E_{kl'}>0} \frac{\left(\phi_{kl}^{\dagger} u_x \phi_{kl'} \right) \left(\phi_{kl'}^{\dagger} u_y(k) \phi_{kl} \right) - \left(\phi_{kl}^{\dagger} u_y(k) \phi_{kl'} \right) \left(\phi_{kl'}^{\dagger} u_x \phi_{kl} \right)}{(E_{kl} - E_{kl'})^2}
\tag{4.42}
$$

4.4 Results

4.4.1 The behavior of the gap

In Figure 4.5 we investigate the behavior of the gap ΔE as a function of the system para-
meters, namely the strength of magnetic field B_0, perpendicular to the tube axis, the strength
of the scalar potential U_0 and the magnetic flux θ treading the tube. We compare the numerical
results and perturbative results to test the accuracy and range of applicability of the pertur-
bative results. The numerical results are indicated by the circles and the solid line shows the
perturbative analytical result. We consider an infinitely long, metallic carbon nanotube.

In (a) and (b) we investigate the case where there is no magnetic flux threading the tube, so
that $\theta = 0$. In (a) the gap between the valence band and the conduction band is plotted as a
function of the magnetic field strength of the magnetic field perpendicular to the tube axis. Here
we choose the scalar potential to be $U_0 = 0.01\ t$. In the limit of weak magnetic field, U_0 has to
be small compared to $\hbar v_F/R$. For the specified scalar potential we calculate $U_0 R/\hbar v_F = 0.09$, so
that the scalar potential is sufficiently small for perturbative theory in U_0 to be accurate. In (b)
the gap is plotted as a function of the scalar potential. We choose the strength of the magnetic
field to be, $B_0 = 0.005\ \hbar/ea^2$. The analytical results and the numerical results agree up to a
value of $U_0 \sim 0.04\ t$. For this value the parameter that controls the accuracy of the perturbation
expansion is $U_0 R/\hbar v_F = 0.37$.

In (c) and (d) the gap is plotted as a function of the magnetic flux. The small magnetic field
limit is considered in (c). We choose $B_0 = 0.005\ \hbar/ea^2$, so that the radius is 0.57 times the
magnetic length. For the specified magnetic field strength, the magnetic length is longer than
the radius and the eigenstates are sensitive to the boundary conditions. The gap has therefore
a strong θ dependence. In the small magnetic field limit, perturbation theory is an accurate
approximation when $\hbar v_F |\boldsymbol{k}|$ is small compared to $\hbar v_F/R$. When $\theta \sim \pm\pi$, we see that the first
order perturbation result does not reproduce the numerical result. The reason for this is that
in this region the perturbation $\hbar v_F \boldsymbol{k} \cdot \boldsymbol{\sigma}$ that depends on θ (see Equation (3.40)) becomes too
large for first order perturbation results to be accurate. In (d) we choose the magnetic field
$B_0 = 0.05\ \hbar/ea^2$ so that the ratio $R/l_m = 1.8$ corresponds to the large magnetic field regime.
Here the radius is longer than the magnetic length and because the eigenstates are localized on
the scale of the magnetic length, they become insensitive to the boundary conditions and the
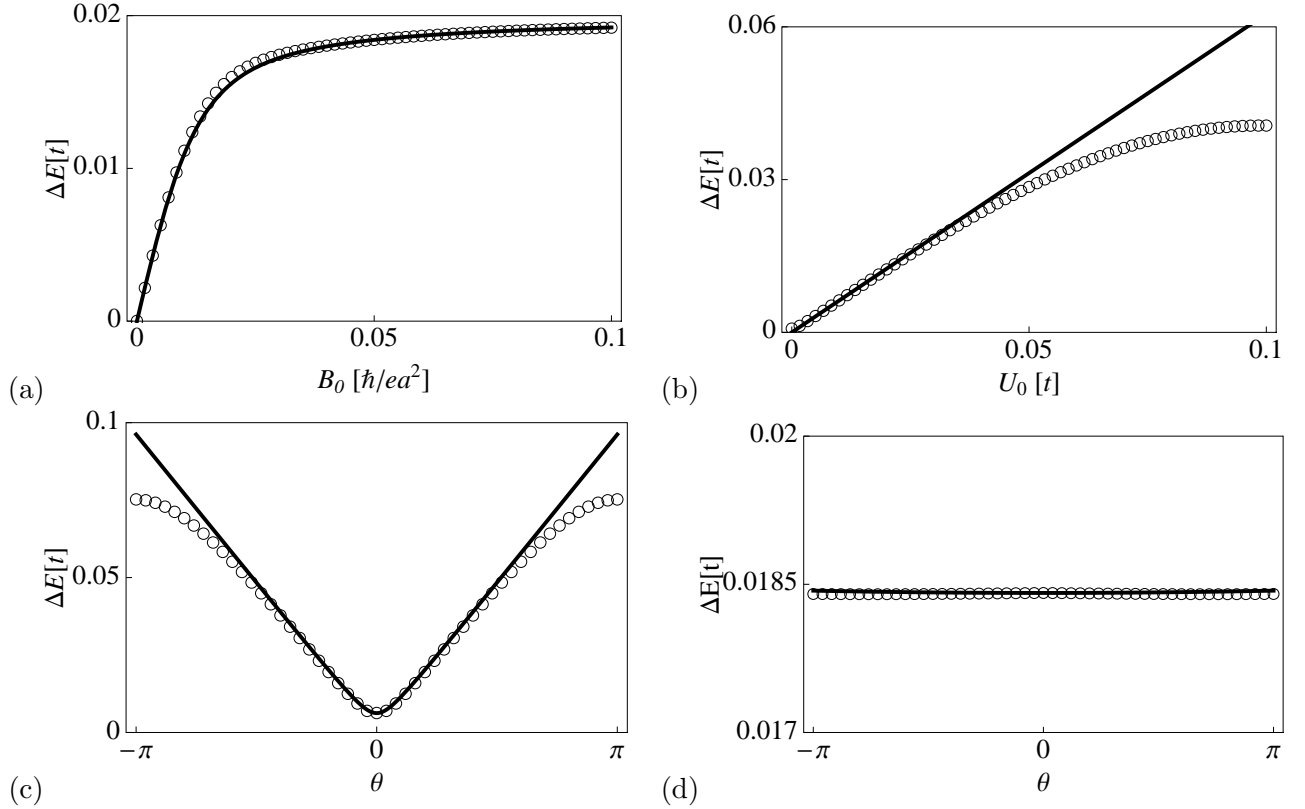gap is independent of θ.

(a)   (b)   (c)   (d)

Figure 4.5: **The behavior of the gap between the valence band and the conduction band as a function of the system parameters. The solid lines are obtained from the analytical calculations and the circles are the numerical results obtained by diagonalizing the nearest neighbor tight binding Hamiltonian of the carbon nanotube system. (a) The gap ΔE versus the strength of the magnetic field perpendicular to the tube axis. The strength of the scalar potential is $U_0 = 0.01\ t$. In (a) and (b) there is no flux through the tube. (b) The gap ΔE versus the strength of the scalar potential. The strength of the magnetic field is $B_0 = 0.005\ \hbar/ea^2$. (c), (d) The gap ΔE as a function of the magnetic flux through the tube. The strength of the scalar potential is $U_0 = 0.007\ t$. (c) The magnetic field strength is $B_0 = 0.005\ \hbar/ea^2$. (d) The magnetic field strength is $B_0 = 0.05\ \hbar/ea^2$.**

4.4.2   Hall conductance

We now compare the numerical results of the Hall conductance obtained in this chapter with the analytical results we obtained in the previous chapter. For the numerical results, we consider a zig-zag carbon nanotube that has 4 000 hexagons along the length of the tube. This is equal to a carbon nanotube with a length of $\Lambda = 0.85\ \mu m$. The computational time places a restriction on the radius of the carbon nanotube that can be used in the numerical algorithm. We can perform calculations for $R \lesssim 2$ nm in reasonable time. To obtain a ratio of the order $R/l_m \gtrsim 1$ we then have to consider magnetic fields that are unrealistically large. However, in an experimental setup the radius will be larger, so that realistic values of B_0 can be used to obtain the expected ratio

between the radius and the magnetic length.

In Figure 4.6 we plot the Hall conductance as a function of the magnetic flux. The curves are symmetric about $\pi = 0$, and therefore we do not have to consider the interval between $-\pi$ and 0 but only the interval between 0 and π.

In (a) and (b) we consider the small magnetic field limit i.e. where $R \ll l_m$, for both a metallic and a semi-conducting tube. The analytical results of Equation (3.71) are represented by the solid line. The small γ approximation of a single Lorentzian peak is represented by the dashed line while the circles represents the numerical results. In both (a) and (b) we choose $U_0 = 0.01$ t and $B_0 = 0.005\ \hbar/ea^2 \simeq 53\ T$. In (a) we consider a metallic tube. For metallic tubes the index ν is equal to zero and we therefore choose the radius $R = 51\ a/2\pi$, so that $\nu = 51 \bmod 3 = 0$. For the specified magnetic field, the ratio between the radius and the magnetic length is small, $R/l_m = 0.57$. As expected, we see a Lorentzian peak at $\theta = 0$. In (b) we consider a semi-conducting tube. For a semi conducting tube the index ν should be equal to ± 1. We therefore choose the radius $R = 50a/2\pi$, so that $\nu = 50 \bmod 3 = -1$. Again $R/l_m = 0.56$ is small. Lorentzian peaks are observed at $\theta = \pm 2\pi/3$. In the small magnetic field limit, good agreement between the analytical and numerical results exists for both the metallic tube and the semi-conducting tube.

In (c) and (d) we investigate a semi-conducting tube in the intermediate and strong magnetic field regime, respectively. In both cases we choose $U_0 = 0.007\ t$ and the radius as $R = 50a/2\pi$. In (c) we choose $B_0 = 0.015\ \hbar/ea^2$ so that $R/l_m = 0.97$. The analytical results in the intermediate magnetic field regime do not reproduce the numerical results as well as in the small magnetic field regime. The reason for this is as follows. For the specified magnetic field strength, the level spacing of the zero order Hamiltonian, Equation (2.45a), is of the same order as the perturbation for some modes that contribute to the Hall conductance. In (d) we choose the magnetic field to be $B_0 = 0.05\ \hbar/ea^2$ and the ratio between the radius and the magnetic field equal to $R/l_m = 1.8$. Good agreement between the analytical and numerical results exits in the strong magnetic field regime. This is a result of the eigenstates being localized on the scale of the magnetic length l_m and the fact that the magnetic flux θ only appears in the boundary condition. Therefore, in the strong magnetic field regime, the eigenstates become insensitive to the boundary condition and is independent of θ. The Hall conductivity is quantized to e^2/h per spin independent of θ.

In conclusion, a comparison between the numerical and analytical results indicate that the analytical results are most accurate in the limits of small and large magnetic length and less accurate for $l_m \simeq R$. However, the average of the Hall conductance over θ is always quantized as e^2/h.
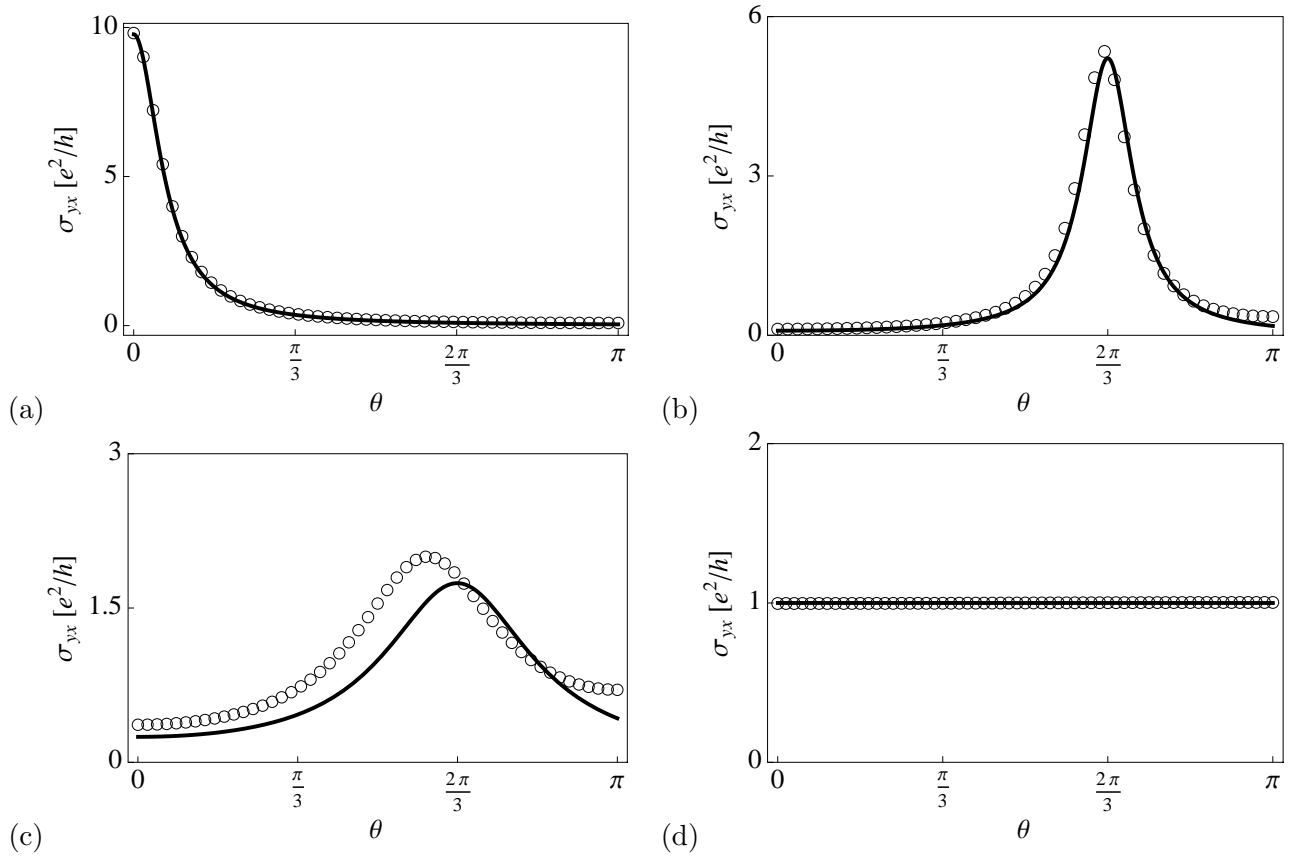
Figure 4.6: The Hall conductivity σ_{yx} as a function of the magnetic flux θ. The analytical results are indicated by the solid line, and the numerical results by the circles. (a) **A carbon nanotube with 51 hexagons around the circumference and subjected to a magnetic field and electric field parallel to the tube axis, so that the strength of the magnetic field is $B_0 = 0.005\ \hbar/ea^2$ and the strength of the vector potential is $U_0 = 0.001\ t$.** (b) **The parameters are the same as in (a), but here we investigate a carbon nanotube that has 50 hexagons around the circumference, i.e. we investigate a semi-conducting carbon nanotube.** (c) **The magnetic field is chosen to be in the intermediate regime. The semi-conducting carbon nanotube subjected to a magnetic field and electric field, so that $B_0 = 0.015\ \hbar/ea^2$ and $U_0 = 0.007\ t$.** (d) **Here the magnetic field is in the strong magnetic field regime, the carbon nanotube is subjected to a magnetic field with a strength $B_0 = 0.005\ \hbar/ea^2$ and scalar potential $U_0 = 0.007\ t$.**

CHAPTER 5
Results

The conclusions reached in the earlier chapters are summarized in this chapter. I formulate the conclusions in terms of questions followed by answers.

5.1 Is a gap in the electronic spectrum of a previously metallic carbon nanotube induced?

In the absence of any external field the valence band and the conductance band of a metallic carbon nanotube touch at the two inequivalent Dirac points, K and K'. If apply we a constant magnetic field perpendicular to the axis of the carbon nanotube, a gap between the valence band and the conductance band is induced, Landau levels are formed and a quantized Hall conductance is expected. If the constant magnetic field is now replaced with an magnetic field that averages to zero around the edge of the carbon nanotube, the valence band and the conduction band touch, as in the case where the magnetic field is absent. However, we observe two interesting features due to the magnetic field. Firstly, we see that the Fermi velocity of the states around the Dirac points is reduced. Secondly, due to time reversal symmetry breaking, the degeneracy of higher and lower energy subbands is lifted (see Figure 3.4).

There exists two zero energy eigenstates. One of them confines the electrons of the A sublattice in the K valley and the electrons of the B sublattice in the K' valley to regions where the magnetic field points in the positive z-direction. The other state does exactly the opposite. It confines electrons of the A sublattice in the K' valley and electrons of the B sublattice in the K valley to regions where the magnetic field points in the negative z-direction. If we apply an electrostatic potential that is either correlated or anti correlated with the magnetic field, a gap is induced in the electronic spectrum of the carbon nanotube. If these fields are anticorrelated, the valence band states are confined in regions where the magnetic field is positive. When the fields are correlated, the valence band states are confined to regions where the magnetic field is negative. As a result, the valence-band electrons experience a magnetic field with a nonzero average even though the magnetic field averages to zero over the carbon nanotube sample as a whole.

To answer the question stated above: Yes, in the presence of parallel magnetic and electric fields that are perpendicular to the carbon nanotube axis (that was previously metallic) devel-

ops a gap. However, gap formation in the electronic spectrum of a previously metallic carbon nanotube does not secure a quantized Hall conductance.

5.2   Do we observe a quantized Hall conductance?

We started with the Kubo formula and derived an analytical expression for the Hall conductance when the Fermi energy is in the gap. The expression is given by Equation (3.71):

$$\sigma_{yx} = \frac{e^2}{h} \sum_m \left[\frac{\gamma}{\gamma^2 + (2\pi m + \theta - 2\pi\nu/3)^2} + \frac{\gamma}{\gamma^2 + (2\pi m + \theta + 2\pi\nu/3)^2} \right], \qquad (5.1)$$

where $\gamma = 2\pi R\mu/\hbar\tilde{v}_F$. To obtain this result we had to make the following assumptions:

1. The first order perturbation theory in k and U_0 is sufficiently accurate for all the modes that contribute to the Hall conductance.

2. All the modes for which first order perturbation theory is inaccurate and that is included in the sum of the analytical expression for the Hall conductance, give a negligible contribution.

To test if these assumptions place a restriction on the strength of the magnetic field, we compared the analytical expression with numerical results obtained by diagonalizing the nearest neighbor tight binding Hamiltonian. The range of applicability of the magnetic field is tested by investigating the Hall conductance in the following regions: small, intermediate and large radius to magnetic length ratios, i.e. R/l_m.

A comparison between the analytical results and numerical calculations indicate that the analytical results reproduce the numerical results very well in the limits of small or large R/l_m, but is less accurate for intermediate values. The reason for the less accurate reproduction of the result is due to the level spacing of the zero order Hamiltonian that is of the same order as the perturbation for some modes that contribute to the Hall conductance.

We arrived at the following result concerning the question above: the average of the Hall conductance as a function of θ over θ, i.e.

$$\langle \sigma_{yx} \rangle_\theta = \int_0^{2\pi} d\theta \, \sigma_{yx}(\theta)/2\pi. \qquad (5.2)$$

is always quantized: $\langle \sigma_{yx} \rangle_\theta$ equals $\pm 2e^2/h$ (factor 2 for spin). This is true for all three regions - small medium and large radius to magnetic length ratios.

5.3 Does there exists a connection between the Hall conductance observed in a quasi-one dimensional system and topological invariants?

Yes, as explained in Chapter 2, an argument that connects the Hall conductance with a topological invariant is provided by Niu, et al. However, this argument does not guarantee a quantized Hall conductance in our system. It only guarantees that when the flux threading the tube is varied by one flux quantum, an integer amount of electrons is transported from the one side of the tube to the other. The argument does not exclude the trivial case of zero electrons transported. We therefore ask the question in the following section:

5.4 What is the current I that flows along the axis of the tube when the flux is varied by one flux quantum?

The non-zero Hall conductance and the quantization of its average can be observed when we vary the flux, Φ, threading the tube. We found that one electron per spin is transported through the tube as we vary the flux by one flux quantum.

An overview of the conclusion: we derived an expression for the Hall conductance when the Fermi energy is in the gap. This expression agrees well with numerical results obtained from the nearest neighbor tight binding Hamiltonian. The non-zero Hall conductance leads to quantized transport and when the flux through the tube is varied by one flux quantum, exactly one electron per spin is transported between the ends of the tube.

BIBLIOGRAPHY

[1] D.C. Giancoli, *Physics*, Prentice Hall, New Jersey (1998).

[2] M. Stone, *The Quantum Hall Effect*, World Scientific, Singapore (1992).

[3] G. Landwehr, Metrologia, **22** (1986).

[4] D. Yoshioka *The Quantum Hall Effect*, Springer, Germany (2002).

[5] K. v. Klitzing, G. Dora, and M. Pepper, Phys. Rev. Lett. **45**, 494 (1980).

[6] S. Das Sarma, A. Pinczuk, *Perspectives in Quantum Hall Effects*, Wiley, New York (1997).

[7] T. Morimoto, Y. Hatsugai, H. Aoki, Phys. Rev. Lett. **103**, 116803 (2009).

[8] D. Thouless, M. Kohmoto, M. Nightingale, M. den Nijs, Phys. Rev. Lett. **49**, 405 (1982).

[9] J. Bellissard, A. van Elst, H. Schultz-Baldes, J. Math. Phys. **35**, 5373 (1994).

[10] J.E. Avron, D. Osadchy, R. Seiler, Phys. Today **56**, 38 (2003).

[11] C.L. Kane and E.J. Mele, Phys. Rev. Lett. **95**, 226801 (2005).

[12] F.D.M. Haldane, Phys. Rev. Lett. **61**, 2015 (1988).

[13] K.S. Novoselov, Z. Jiang, Y. Zhang, S.V. Morozov, H.L. Stormer, U. Zeitler, J.C. Maan, G.S. Boebinger, P. Kim, A.K. Geim, Science **315**, 1379 (2007).

[14] I. Snyman, Phys. Rev, B **80**, 054303 (2009).

[15] Q. Niu, D.J. Thouless and Y-S Wu, Phys. Rev, B **31**, 3372 (1985).

[16] P.R. Wallace, Phys. Rev. **71**, 662 (1947).

[17] J.W. McClure, Phys. Rev. **104**, 666 (1956).

[18] K.S. Novoselov, A.K. Geim, S.V. Morozov, D. Jiang, Y. Zhang, S.V. Dubonos, I.V. Grigorieva and A.A. Firsov, Sience **306**, 666 (2004).

[19] A.K. Geim, K.S. Novoselov, Nature Mater. **6**, 183 (2007).

[20] N.W. Ashcroft, N.D. Mermin, *Solid State Physics*, Saunders College, Philadelphia (1976).

[21] A.H. Castro Neto, F. Guinea, N.M.R. Peres, K.S. Novoselov, and A.K. Geim, Reviews of Modern Physics, **81**, 109 (2009).

[22] N.M.R. Peres, Europhys. News, **40**, 17 (2009).

[23] C. W. J. Beenakker, Rev. Mod. Phys. **80**, 1337 (2008).

[24] T. Ando, J. Phys. Soc. Jpn. **74**, 777 (2005).

[25] T. Ando ,Y. Matsumoto and Y. Uemura J . Phys. Soc. Japan **39** 279 (1975).

[26] A. Kanda, S. Uryu, K. Tsukagoshi, Y. Ootuka, and Y. Aoyagi, Physica B **323**, 246 (2002).

[27] A. Bachtold, C. Strunk, J. Salvetat, J. Bonard, L. Forro, T. Nussbaumer, and C. Schonenberger, Nature **397**, 673 (1999).

[28] A. Bourlon, C. Miko, L. Forro, D.C. Glattli, and A. Bachtold, Phys. Rev. Lett. **93**, 176806 (2004).

[29] J. Cumings and A. Zettl, Phys. Rev. Lett., **93**, 086801, (2004).

[30] J. Cumings, A. Zettl, Science, **289**, 602 (2000).

[31] R. B. Laughlin, Phys. Rev. B, **23**, 5632 (1981).

[32] C-H Park, L.Z. Tan, S.G. Louie, Physica E, **43**, 651 656 (2011).

[33] M.R. Masir, P. Vasilopoulos, F.M. Peeters, J. Phys. Condens. Matter **22** 465302 (2010).

[34] Y. Zhang, Y.W. Tan, H.L. Stormer and P. Kim, Nature, **438**, 201 (2005).